HETEROGENEOUS EXPECTATIONS WITH MULTIPLE RISKY ASSETS

Documents de travail GREDEG
GREDEG Working Papers Series

Riccardo Sommariva
Paolo Zeppini

GREDEG WP No. 2026-18
https://ideas.repec.org/s/gre/wpaper.html

Heterogeneous Expectations with Multiple Risky Assets

Sommariva R.[1] and Zeppini P.[1]

[1]Université Côte d'Azur, CNRS, GREDEG, France

GREDEG Working Paper No. 2026-18

Abstract

We extend the heterogeneous agent model of Brock and Hommes (1997, 1998) to a setting with two risky assets. Agents choose between a trend-following rule and a fundamentalist rule using evolutionary switching based on past performance. The expectation rules operate on both assets simultaneously: the forecast for each asset depends on the lagged price deviation of the other, introducing cross-asset expectations as a new channel for endogenous comovement. In the deterministic skeleton we derive the threshold intensity of choice at which the fundamental steady state loses stability and show that cross-asset expectations lower it: the fundamental steady state destabilizes sooner, and the interval of stable non-fundamental dynamics that follows shrinks. In the stochastic system, they amplify the realized correlation far beyond the exogenous baseline: as the intensity of switching approaches the pitchfork threshold the realized correlation approaches one, however weakly the two fundamentals are correlated. This amplification is non-monotonic in the intensity of choice and it operates through the structure of expectations alone.

Keywords: Heterogeneous agent model, Excess comovement, Cross-asset expectations, Multi-asset markets, Nonlinear dynamics.
JEL: G12, D84, C62.

1 Introduction

Empirical asset prices often comove more strongly than fundamentals can explain. Across largely unrelated markets, price covariation persists after conditioning on all observable macroeconomic factors, as systematically documented by Pindyck and Rotemberg (1990) for raw commodities and Pindyck and Rotemberg (1993) for the stock prices of firms in unrelated lines of business, who found excess comovement of returns after conditioning on a present value model with macro-driven discount rates. The comovement to be explained is often neither constant nor uniform. Longin and Solnik (1995) estimate a multivariate GARCH model on monthly excess reurns for different equity markets over $1960 - 1990$ and show how correlations inrcease over the three decades and rise in periods of high market volatility.

These patterns have motivated a large theoretical literature on mechanisms that can decouple price comovement from fundamental comovement. Barberis et al. (2005) argue that when investors group assets into categories, or respond to common sentiment, their correlated demand shifts generate non-fundamental comovement that a frictionless pricing model cannot account for. A separate mechanism is informational rather than behavioral: Veldkamp (2006) shows that when information is costly to acquire but cheap to reproduce, investors purchase signals about a subset of assets and pricing many assets with that information produces price covariance in excess of fundamental covariance. The question that follows is whether expectation formation, independently of portfolio rebalancing or sentiment shocks, can be a source of excess comovement and whether such mechanism can be studied in a tractable framework.

Heterogeneous agent models (HAMs) make expectation formation itself the object of study, though most of this literature considers a single risky asset market. The seminal contributions of Brock and Hommes (1997, 1998) establish the building block: agents choose among a finite set of forecasting rules on the basis of past performance, and the resulting nonlinear feedback between beliefs and prices generates rich endogenous dynamics, including bifurcation routes to cycles and chaos, even when the dividends are IID and the fundamental value is constant. This framework has been shown to reliably reproduce a set of empirical regularities like excess volatility, volatility clustering, temporary bubbles and crashes, short-run momentum and long-run reversal, and to connect these phenomena to the bifurcation structure of the underlying deterministic skeleton; see the surveys of Hommes (2006), Dieci and He (2018) and He et al. (2019). Its two behavioral ingredients, coordination on a common rule and trend extrapolation, have direct experimental support. In the learning-to-forecast design of Hommes et al. (2005), participants' forecasts differ significantly from the constant fundamental and more notably groups coordinate on a common, often trend-following prediction rule.

Trend extrapolation is also the engine of the leading modern account of bubbles: in Barberis et al. (2018), extrapolators weigh a trend signal from past price changes against a measure of overvaluation generating bubbles and volume that rises with past returns.

Comovement, however, is only defined once there is more than one asset, and the multi-asset case has received less attention so far. One of the main challenges in moving to multiple assets is that comovement can arise through several distinct channels, and isolating each requires deliberate modelling choices. Early contributions established that portfolio-based interaction is already sufficient to transmit dynamics across markets. Chiarella et al. (2005) develop a two-risky-asset mean variance model in which heterogeneous agents hold time varying beliefs about expected returns and the variance-covariance structure; changes in beliefs in one market spill over into the other through the portfolio optimization problem. Chiarella et al. (2007) extend this approach and emphasize that once multiple risky assets are available, beliefs about the joint distribution of returns become endogenous objects that drive asset interdependence in ways that have no single-asset analogue. In both models the price forecasts are formed asset by asset and the coupling operates through the covariance matrix entering mean-variance demand. Chiarella et al. (2013) develop the same framework into a boundedly rational equilibrium with time varying betas in which systematic movements of the market portfolio arise independently of fundamentals.

A different comovement mechanism arises from market selection: in Westerhoff (2004) chartists switch between markets based on trend signals, and this mobility alone generates endogenous comovement without any direct portfolio linkage between the assets. The same mechanism operates in Dieci and Westerhoff (2006), where agents move between markets according to relative profitability and in Dieci and Westerhoff (2010); Schmitt and Westerhoff (2014), where stock markets are connected through a foreign exchange market or through direct cross-market spillovers.

From an equilibrium perspective, Anufriev et al. (2012) show that evolutionary pressure toward riskier portfolios in a multi-asset model produces excess covariance in prices relative to dividends, providing a microfoundation for the empirical excess comovement observation. Most closely related to the present paper, Hommes and Vroegop (2019) introduce a two market model in which the markets are linked through a bias term in the chartists' forecasting rule that depends on the deviation in the other market, generating destabilizing spillovers and comovement through a cross market belief channel. Despite the richness of this literature, the cross market link enters either through portfolio mechanics, through the switching mechanism or as a scalar perturbation to an otherwise market specific forecasting rule. To our knowledge, no existing model specifies the forecasting rule itself as a joint object defined over both assets simultaneously.

The present paper introduces this structure as a distinct channel: cross-asset expectations. We develop a two asset HAM in which agents choose between a trend-following rule and a fundamentalist rule, as in Brock and Hommes (1998), but the trend-following rule operates on both assets simultaneously through a forecasting matrix, whose off-diagonal elements allow the past mispricing of one asset to enter the forecast for the other, capturing the idea that expectations are partly shaped by cross-asset price information. This generalizes the scalar cross-market bias of Hommes and Vroegop (2019) to a full set of cross-asset forecasting coefficients.

Such cross-asset signals are widely present in practice: pairs trading defines positions explicitly on the joint behavior of two assets' prices (Gatev et al., 2006), and timeseries momentum is documented across equity index, currency, commodity and bond futures with cross-asset correlations that exceed those of the underlying assets themselves (Moskowitz et al., 2012), making it natural to model trend-following as a joint rule rather than a collection of independent single asset rules. Under the zero net supply assumption, the fundamental correlation drops out of the pricing equations (Appendix B), so the deterministic model isolates the expectation channel analytically making the framework a good candidate to study the emergence of endogenous correlation.

We analyze the model in two stages. In the deterministic skeleton, cross-asset expectations lower the stability threshold of the fundamental steady state and compress the bifurcation structure: even small off-diagonal elements substantially reduce the parameter region over which the fundamental equilibrium or a stable non-fundamental fixed point can persist. In the stochastic system, cross-asset expectations amplify the realized correlation between the two price deviations far beyond the exogenous noise correlation. The resulting realized correlation is non-monotone in the intensity of switching, and we trace this non-monotonicity to the eigenvalue structure of the Jacobian at the non-fundamental fixed point.

The paper is organized as follows. Section 2 presents the model; Section 3 derives the stability conditions for the fundamental steady state; Section 4 explores the deterministic skeleton numerically; Section 5 analyzes the stochastic system; Section 6 concludes.

2 The model

Consider a market with two risky assets and one risk-free asset. Asset 1 has price p_t and pays dividend d_t; asset 2 has price q_t and pays dividend c_t. The risk-free asset yields a gross return $R \equiv 1 + r$. A population of N investors, indexed by expectation type $h = 1, \ldots, H$ with $H < N$, allocates wealth W_t across the three assets. Denoting by z_t and v_t, the shares held in the two risky assets, next-period wealth is

$$W_{t+1} = W_t R + z_t(p_{t+1} + d_{t+1} - Rp_t) + v_t(q_{t+1} + c_{t+1} - Rq_t).$$

Each investor of type h maximizes mean-variance utility

$$\max_{z_t, v_t} U_{ht} = \mathrm{E}_{ht}[W_{t+1}] - \frac{1}{2} a \,\mathrm{Var}_{ht}[W_{t+1}], \tag{1}$$

where $a > 0$ is a common coefficient of absolute risk aversion. As in Brock and Hommes (1998), we impose three simplifying assumptions: (i) risk aversion is homogeneous, $a_h = a$ for all h; (ii) conditional variances are homogeneous and constant; and (iii) conditional covariance is homogeneous and constant. Formally, for all h and all t,

$$\mathrm{Var}_{ht}[p_{t+1} + d_{t+1}] = \sigma_R^2, \qquad \mathrm{Var}_{ht}[q_{t+1} + c_{t+1}] = \sigma_G^2,$$
$$\mathrm{Cov}_{ht}[p_{t+1} + d_{t+1}, q_{t+1} + c_{t+1}] = \rho\, \sigma_R \sigma_G,$$

where $\rho \in (-1, 1)$ is the fundamental correlation between the two assets. The first-order conditions of (1) yield optimal demands (see Appendix A):

$$\begin{cases} z_{ht} = \dfrac{E_{ht}[p_{t+1} + d_{t+1}] - Rp_t - a\rho\sigma_R\sigma_G v_{ht}}{a\sigma_R^2}, \\ v_{ht} = \dfrac{E_{ht}[q_{t+1} + c_{t+1}] - Rq_t - a\rho\sigma_R\sigma_G z_{ht}}{a\sigma_G^2}. \end{cases} \tag{2}$$

Let $n_h t$ denote the fraction of agents using expectation rule h at time t, with $\sum_{h=1}^{H} n_{ht} = 1$. Total supplies of the two assets are z_S and v_S respectively. Imposing market clearing, $\sum_h n_{ht} z_{ht} = z_S$ and $\sum_h n_{ht} v_{ht} = v_S$, and solving for prices gives

$$\begin{cases} p_t = \dfrac{1}{R} \displaystyle\sum_h n_{ht}\, \mathrm{E}_{ht}[p_{t+1} + d_{t+1}] - \dfrac{a\sigma_R}{R}(z_S + \rho\sigma_G v_S), \\ q_t = \dfrac{1}{R} \displaystyle\sum_h n_{ht}\, \mathrm{E}_{ht}[q_{t+1} + c_{t+1}] - \dfrac{a\sigma_G}{R}(v_S + \rho\sigma_R z_S). \end{cases}$$

Following Brock and Hommes (1998), we set $z_S = v_S = 0$. As shown in Appendix B, under zero net supply the terms involving ρ cancel exactly, so the pricing equations reduce to

$$p_t = \frac{1}{R} \sum_h n_{ht}\, \mathrm{E}_{ht}[p_{t+1} + d_{t+1}], \qquad q_t = \frac{1}{R} \sum_h n_{ht}\, \mathrm{E}_{ht}[q_{t+1} + c_{t+1}]. \tag{3}$$

The fundamental correlation ρ therefore plays no role in the pricing equations.

2.1 Heterogeneous expectations

Each type h forms expectations as deviations from the fundamental benchmark. Let p_t^* and q_t^* denote the fundamental prices, $p_t^* = R^{-1}\,\mathrm{E}_t[p_{t+1}^* + d_{t+1}]$ and $q^* = R^{-1}\,\mathrm{E}_t[q_{t+1}^* + c_{t+1}]$. We write

$$\mathrm{E}_{ht}[p_{t+1} + d_{t+1}] = \mathrm{E}_t[p_{t+1}^* + d_{t+1}]f_{ht}, \qquad \mathrm{E}_{ht}[q_{t+1} + c_{t+1}] = \mathrm{E}_t[q_{t+1}^* + c_{t+1}]g_{ht},$$

where f_{ht} and g_{ht} capture the deviation from fundamental expectations. Substituting into (3) and defining the price deviations $\xi_t \equiv p_t - p_t^*$ and $\zeta_t \equiv q_t - q_t^*$, we obtain

$$\xi_t = \frac{1}{R}\sum_h n_{ht} f_{ht}, \qquad \zeta_t = \frac{1}{R}\sum_h n_{ht} g_{ht}. \tag{4}$$

The central modelling choice of this paper is that each forecasting rule operates on both assets simultaneously. Specifically, the belief deviations $(f_{ht}, g_{ht})'$ are linear functions of lagged price deviations in both markets:

$$\begin{pmatrix} f_{ht} \\ g_{ht} \end{pmatrix} = \underbrace{\begin{pmatrix} \phi_{11}^h & \phi_{12}^h \\ \phi_{21}^h & \phi_{22}^h \end{pmatrix}}_{\equiv\, \mathbf{\Phi}^h} \begin{pmatrix} \xi_{t-1} \\ \zeta_{t-1} \end{pmatrix}. \tag{5}$$

The diagonal entries ϕ_{11}^h and ϕ_{22}^h govern own-asset extrapolation: positive values correspond to trend following, negative values to contrarian beliefs, and zero to fundamental expectations. The off-diagonal entries ϕ_{12}^h and ϕ_{21}^h introduce *cross-asset feedback*: they allow the past deviation of one asset to enter the forecast of the other. This is the channel through which non-fundamental correlation between asset prices arises endogenously.

This structure differs from the two-asset framework of Hommes and Vroegop (2019), where the two markets are treated as distinct and expectations in each market depend only on that market's own past prices. In our formulation, a single matrix $\mathbf{\Phi}^h$ governs forecasts for both assets, and the fractions n_{ht} are common across markets: when an agent adopts rule h, it applies to both assets simultaneously.

Parametric cases. The space of expectation matrices can be restricted to economically meaningful specifications. We focus on $H = 2$ throughout, with a trend-following rule $\mathbf{\Phi}^1$ competing against a fundamentalist rule $\mathbf{\Phi}^2 = \mathbf{0}$. Several cases are of interest.

A symmetric trend-following rule with cross asset feedback parametrized by a single scalar φ takes the form

$$\mathbf{\Phi}^1 = \begin{pmatrix} 1 & \varphi \\ \varphi & 1 \end{pmatrix}, \qquad \mathbf{\Phi}^2 = \mathbf{0}.$$

The eigenvalues of $\mathbf{\Phi}^1$ are $1+\varphi$ and $1-\varphi$, so the trend-following rule is non-stationary in isolation. When $\varphi > 0$, the rule expresses a positive cross-asset extrapolation; when $\varphi < 0$, it expresses anti-correlation.

2.2 Performance measure and dynamics of shares

In each period agents evaluate forecasting rules on the basis of past realized profits. Denoting $\boldsymbol{x}_t = (\xi_t, \zeta_t)'$ and the demand vector of type h by $\boldsymbol{k}_{ht} = (z_{ht}, v_{ht})'$, the realized profit of strategy h at time t is

$$\pi_{ht} = \boldsymbol{k}'_{ht-1}(\boldsymbol{x}_t - R\boldsymbol{x}_{t-1}), \tag{6}$$

where $\boldsymbol{x}_t - R\boldsymbol{x}_{t-1}$ is the vector of excess returns on the two assets in terms of deviations (see Appendix C for a decomposition). In the zero-supply, homogeneous-variance setting with $\sigma_R^2 = \sigma_G^2 = \sigma^2$ and $\rho = 0$, the optimal demand of type h at time t reduces to

$$\boldsymbol{k}_{ht} = \frac{1}{a\sigma^2}(\mathbf{\Phi}^h \boldsymbol{x}_{t-1} - Rx_t).$$

Combining with (6), the profit of strategy h at time t is

$$\pi_{ht} = \frac{1}{a\sigma^2}(\mathbf{\Phi}^h \boldsymbol{x}_{t-2} - R\boldsymbol{x}_{t-1})'(\boldsymbol{x}_t - R\boldsymbol{x}_{t-1}). \tag{7}$$

The net utility of strategy h is $U_{ht} = \pi_{ht} - C_h$, where $C_h \geq 0$ is an information cost. Following Brock and Hommes (1998), trend-following rules are costless ($C_1 = 0$), while the fundamentalist rule requires paying a cost $C_2 = C > 0$ to observe the fundamental price.

Agents choose among rules according to a discrete-choice model (McFadden 1981; Brock and Durlauf 2001). The fraction of agents adopting rule h at time t is

$$n_{ht} = \frac{\exp\left(\beta U_{ht-1}\right)}{\sum_{j=1}^{H} \exp\left(\beta U_{jt-1}\right)}, \tag{8}$$

where $\beta \geq 0$ is the *intensity of switching*. When $\beta = 0$, agents distribute uniformly across rules; as $\beta \to \infty$, all agents coordinate on the best-performing rule.

For $H = 2$ it is convenient to work with the share difference $m_t \equiv n_{1t} - n_{2t}$, which satisfies

$$m_t = \tanh\left(\frac{\beta}{2}\left(U_{1t-1} - U_{2t-1}\right)\right). \tag{9}$$

The system (4)-(9), together with the expectation structure (5) and the profit measure (7), defines a six-dimensional nonlinear map, whose properties we study in next sections.

3 Stability analysis

In this section we discuss the full dynamical system which is represented as a first-order map on $\mathbb{R}^6$ and derive the local stability conditions of the fundamental steady state as close form bound on the intensity of switching β, which shrinks with the off-diagonal elements of the trend-following matrix $\mathbf{\Phi}^1$, destabilizing the fundamental steady state.

3.1 The dynamical system

Substituting the expectation structure (5) into the pricing equations (4) yields the law of motion for the price deviations. Together with the logit switching rule (8) and the profit measure (7), the complete deterministic system is

$$\begin{cases} \xi_t = \dfrac{1}{R}\displaystyle\sum_h n_{ht}(\phi^h_{11}\xi_{t-1} + \phi^h_{12}\zeta_{t-1}), \\ \zeta_t = \dfrac{1}{R}\displaystyle\sum_h n_{ht}(\phi^h_{21}\xi_{t-1} + \phi^h_{22}\zeta_{t-1}), \\ n_{ht} = \dfrac{\exp(\beta U_{ht-1})}{\sum_j \exp(\beta U_{jt-1})}, \\ U_{ht-1} = \boldsymbol{k}'_{ht-2}(\boldsymbol{x}_{t-1} - R\boldsymbol{x}_{t-2}) - C_h. \end{cases} \tag{10}$$

The first two equations are the pricing equations (3) written in terms of the expectation coefficients ϕ^h_{ij}: each price deviation is a discounted weighted average of the forecasting rules, as in Brock and Hommes (1998). The third and fourth equations govern the evolution of the population shares through the logit rule (8) and the performance measure (7).

Because the utility U_{ht-1} depends on $\boldsymbol{x}_{t-1}, \boldsymbol{x}_{t-2}$ and, through the demand $\boldsymbol{k}_{ht-2}$ on $\boldsymbol{x}_{t-3}$, the system involves lags up to order three in each price deviation. To cast it as a first order map we introduce four auxiliary variables, $\gamma_t = \xi_{t-1}$, $\tau_t = \gamma_{t-1}$, $\psi_t = \zeta_{t-1}$, $\mu_t = \psi_{t-1}$, obtaining a six-dimensional state vector

$$\boldsymbol{s}_t \equiv (\xi_t, \gamma_t, \tau_t, \zeta_t, \psi_t, \mu_t)' = F(\boldsymbol{s}_{t-1}), \tag{11}$$

where $F\colon \mathbb{R}^6 \to \mathbb{R}^6$ is the map defined by (10) together with the identity relations for the auxiliary variables.

3.2 The Fundamental Steady State

The *Fundamental Steady State* (FSS) is the fixed point $\boldsymbol{s}^* = \mathbf{0}$, at which prices are set at their fundamental value ($\xi = \zeta = 0$) and all lagged deviations vanish.

At this point profits are zero for every strategy, so the logit fractions reduce to

$$n_h = \frac{\exp(-\beta C_h)}{\sum_j \exp(-\beta C_j)}.$$

For $H = 2$ with $C_1 = 0$ (trend followers) and $C_2 = C > 0$ (fundamentalists), we have $n_1^{FSS} = 1/(1 + e^{-\beta C})$, representing the share of trend-following traders, and $n_2^{FSS} = 1 - n_1^{FSS}$, the share of fundamentalist traders.

At $\boldsymbol{s}^* = \mathbf{0}$ every strategy earns zero profit and the net utilities differ only by the information cost. If $C_2 = 0$ the two types split evenly, $n_1^{FSS} = n_2^{FSS} = \frac{1}{2}$ for every β. When $C_2 > 0$, the share of the costly fundamentalist strategy, $1/(1 + e^{\beta C})$, decreases monotonically to zero as β increases: no agent pays to use the fundamentalist strategy in a steady state where doing so yields no extra profit, and faster selection concentrates mass on the strategy that is best in net terms, i.e. the cheapest strategy (Brock and Hommes, 1998).

3.3 Jacobian and eigenvalue reduction

Local stability of the FSS is determined by the eigenvalues of the Jacobian $J = DF(\boldsymbol{s}^*)$. Because the auxiliary variables are lag shifts ($\gamma_t = \xi_{t-1}$, etc.), most rows of J are trivial: evaluated at the FSS, J takes the block form

$$J_{FSS} = \left[\begin{array}{ccc|ccc} a_{11} & 0 & 0 & a_{12} & 0 & 0 \\ 1 & 0 & 0 & 0 & 0 & 0 \\ 0 & 1 & 0 & 0 & 0 & 0 \\ \hline a_{21} & 0 & 0 & a_{22} & 0 & 0 \\ 0 & 0 & 0 & 1 & 0 & 0 \\ 0 & 0 & 0 & 0 & 1 & 0 \end{array}\right], \tag{12}$$

where a_{ij} denotes the non trivial partial derivatives defined below. The companion rows contribute four zero eigenvalues, so local stability is governed entirely by the 2×2 block

$$A \equiv \begin{pmatrix} a_{11} & a_{12} \\ a_{21} & a_{22} \end{pmatrix}, \tag{13}$$

which maps $(\xi_{t-1}, \zeta_{t-1})'$ into $(\xi_t, \zeta_t)'$ at the FSS.

To compute A, note that at the FSS the shares n_h^{FSS} are constants independent of the state (since all profits vanish), so differentiating the pricing equations with respect to the lagged deviations yields

$$a_{ij} = \frac{1}{R} \sum_h n_h^{FSS} \phi_{ij}^h, \qquad i, j \in \{1, 2\}.$$

Each entry of A is a weighted average of the corresponding forecasting coefficients across strategies, discounted by R. In the main case of interest where the fundamentalist rule satisfies $\mathbf{\Phi}^2 = \mathbf{0}$, this simplifies to

$$A = \frac{n_1^{FSS}}{R}\mathbf{\Phi}^1. \tag{14}$$

3.4 Stability conditions

The FSS is locally asymptotically stable if and only if both eigenvalues of A lie strictly inside the unit circle. Since $A = (n_1^{FSS}/R)\mathbf{\Phi}^1$ under (14), its trace and determinant are $T_A = (n_1^{FSS}/R)T$ and $D_A = (n_1^{FSS}/R)^2 D$, where

$$T \equiv \mathrm{Tr}(\mathbf{\Phi}^1) = \phi_{11}^1 + \phi_{22}^1, \qquad D \equiv \mathrm{Det}(\mathbf{\Phi}^1) = \phi_{11}^1\phi_{22}^1 - \phi_{12}^1\phi_{21}^1.$$

Applying the Jury conditions for a second-order characteristic polynomial[1] to the characteristic polynomial of A yields the following result.

Proposition 3.1 (Stability of the FSS)**.** *Let $\mathbf{\Phi}^2 = \mathbf{0}, T > 0, D > 0$, and $\Delta C \equiv C_2 - C_1 > 0$. The FSS is locally asymptotically stable if and only if the share of trend followers satisfies $n_1^{FSS} < n_\mathrm{c}$, where*

$$n_\mathrm{c} \equiv R \min\left\{\frac{1}{\sqrt{D}}, \frac{T - \sqrt{T^2 - 4D}}{2D}\right\} \tag{15}$$

Equivalently, since n_1^{FSS} is striclty increasing in β, the FSS is locally asymptotically stable if and only if

$$\beta < \beta_\mathrm{c} \equiv \frac{1}{\Delta C}\ln\left(\frac{n_\mathrm{c}}{1 - n_\mathrm{c}}\right). \tag{16}$$

Proof. See Appendix D. □

Proposition 3.1 provides a necessary and sufficient condition for the stability of the Fundamental Steady State in terms of the trace and determinant of Φ^1 and therefore covers any 2×2 specification with $T > 0$ and $D > 0$. The *critical threshold* n_c is the maximum share of trend followers compatible with a locally stable FSS: below it, the stabilising effect of fundamentalists is strong enough to anchor prices to fundamentals; above it the FSS loses stability. When $T^2 < 4D$, the eigenvalues of $\mathbf{\Phi}^1$ are complex conjugate, the condition $1 - T_A + D_A > 0$ is automatically satisfied for all positive n_1^{FSS}, and only the third $1 - D_A > 0$ binds; in that case $n_\mathrm{c} = R/\sqrt{D}$. In terms of the switching parameter, β_c is the largest intensity of choice

[1] The Jury conditions state that both roots of $\lambda^2 - T_A\lambda + D_A = 0$ lie inside the unit disc if and only if (i) $1 + T_A + D_A > 0$, (ii) $1 - T_A + D_A > 0$, and (iii) $1 - D_A > 0$.

compatible with FSS stability. For $\beta < \beta_c$ agents respond slowly to the fitness gap, the population remains spread across rules and the fundamentalist share is large enough to stabilize prices; for $\beta > \beta_c$ agents respond sharply and concentrate on the cheaper trend-following rule, pushing n_1^{FSS} above n_c and destabilising the FSS. Note that β_c depends on ΔC: a smaller information cost differential raises β_c, the Fundamental Steady State remains stable for a longer interval when the strategies have similar costs.

Whether a finite β_c exists at all is governed by the spectral radius $\rho(\mathbf{\Phi}^1)$, equal to $\lambda_{\max}$ for real eigenvalues and to $\sqrt{D}$ for complex ones, through $n_c = R/\rho(\mathbf{\Phi}^1)$. Since $n_1^{\mathrm{FSS}}(\beta)$ increases strictly from $\frac{1}{2}$ at $\beta = 0$ to 1 as $\beta \to \infty$, the FSS is stable for every β when $\rho(\mathbf{\Phi}^1) \leq R$, unstable for every $\beta > 0$ when $\rho(\mathbf{\Phi}^1) \geq 2R$ and loses stability at the unique threshold $\beta_c = \Delta C^{-1} \ln\big(R/(\rho(\mathbf{\Phi}^1) - R)\big)$ when $R < \rho(\mathbf{\Phi}^1) < 2R$; the three specifications of Section 4 all fall in this last regime (see Figure 1).

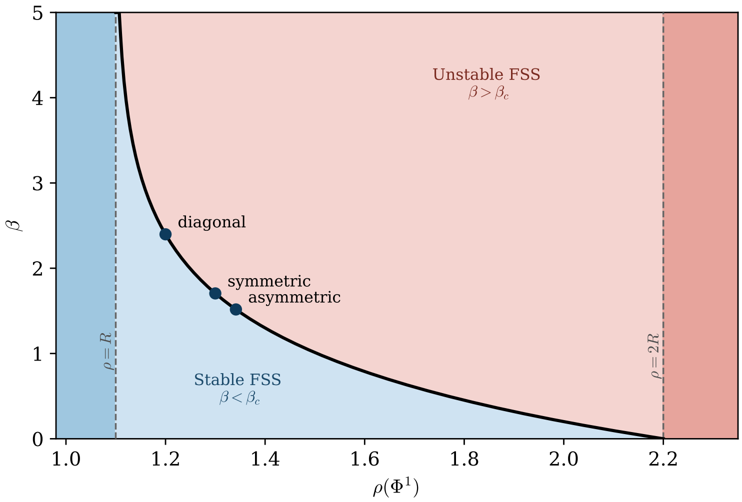

Figure 1: Local stability of the fundamental steady state in the $(\rho(\mathbf{\Phi}^1), \beta)$ plane, for $R = 1.1$, $\Delta C = 1$. The solid curve is the exact boundary $\beta_c(\rho) = \Delta C^{-1} \ln[R/(\rho - R)]$, separating the locally stable region (blue, $n_1^{FSS}(\beta) < R/\rho$) from the unstable one (red). We can identify three regimes that charecterize the stability of the FSS as three columns: for $\rho \leq R$ the FSS is stable for every β; for $R < \rho < 2R$ it loses stability at a single finite β_c; for $\rho \geq 2R$ it is unstable for all $\beta > 0$. The diagonal, symmetric and asymmetric specifications (markers, $\rho = 1.20, 1.30, 1.34$) all lie in the intermediate regime, on a single boundary curve, with $\beta_c = 2.40, 1.70, 1.52$.

An alternative sufficient condition based on the Gershgorin circle theorem, which provides a simpler but more conservative bound, is given in Appendix E.

Baseline example. For the parametrization $R = 1.1, C_1 = 0, C_2 = 1, \mathbf{\Phi}^1 = \mathrm{diag}(1.2, 1.2), \mathbf{\Phi}^2 = \mathbf{0}$, we have $T = 2.4, D = 1.44$, and $T^2 = 4D$. Both bounds in (15) coincide at $n_c = R/\sqrt{D} \approx 0.917$ giving $\beta_c \approx 2.4$. The FSS is therefore locally stable for all $\beta < 2.4$: even though trend followers pay no information cost, the FSS remains stable for moderate values of the intensity of switching. As β increases beyond β_c, the FSS loses stability and non-fundamental dynamics emerge.

Effect of cross-asset feedback. Introducing non-zero off-diagonal elements in $\mathbf{\Phi}^1$ increases $T^2 - 4D$ (when the off-diagonal entries share the same sign) and lowers n_c through the second bound in (15). Cross-asset feedback therefore destabilises the FSS: a smaller intensity of switching suffices to push the system beyond the stability boundary. Quantitatively, for $\mathbf{\Phi}^1 = \left(\begin{smallmatrix} 1.2 & 0.1 \\ 0.1 & 1.2 \end{smallmatrix}\right)$ we obtain $\beta_c \approx 1.7$, and for $\mathbf{\Phi}^1 = \left(\begin{smallmatrix} 1.2 & 0.2 \\ 0.1 & 1.2 \end{smallmatrix}\right)$ the threshold drops further to $\beta_c \approx 1.52$. The mechanism is transparent from (14): larger off-diagonal entries increase the spectral radius of $\mathbf{\Phi}^1$ and hence of A, tightening the stability bound. In Section 4 we investigate the properties of the system beyond the fundmental steady state, classifying the dynamics for each of the three cases above.

4 Numerical analysis

The stability analysis of Section 3 provides conditions under which the fundamental steady state is locally asymptotically stable, expressed through the threshold β_c on the intensity of switching. Beyond this threshold the FSS loses stability: one eigenvalue of the block A crosses $+1$, which, given the symmetry of the FSS ($\mathbf{s}^* = \mathbf{0}$), corresponds to a pitchfork bifurcation. The analytical framework, however, is silent on the global dynamics that emerge past the bifurcation point: the nature of the attractors, the route to complex behaviour, and the comovement properties of the two price deviations. We address these questions by simulating the deterministic skeleton of the system.

Throughout this section the parameters $R = 1.1$, $C_1 = 0$, and $(a\sigma^2)^{-1} = 1$ are held fixed. The fundamentalist rule is $\mathbf{\Phi}^2 = \mathbf{0}$ in all experiments. The objects of interest are the trend-following matrix $\mathbf{\Phi}^1$ and the intensity of switching β. Initial conditions are set to $\xi = 0.1$ and $\zeta = 0.15$.

We proceed in three steps. First, we consider a diagonal $\mathbf{\Phi}^1$ that reduces the model to two decoupled copies of the Brock and Hommes (1998) single-asset framework, linked only through the shared switching mechanism. This serves as the benchmark against which the effects of cross-asset expectations are measured. Second, we introduce symmetric off-diagonal elements in $\mathbf{\Phi}^1$, so that each asset's forecast extrapolates equally from the other. Third, we allow the off-diagonal elements to differ, breaking the exchange symmetry between the two assets.

4.1 Diagonal benchmark

The diagonal benchmark sets off-diagonal entries of $\mathbf{\Phi}^1$ to zero, so that each asset's forecasting rule depends only on its own lagged deviation. The two pricing equations are then decoupled and the model reduces to two independent copies of the single asset framework of Brock and Hommes (1998), sharing only the population shares n_{1t}, n_{2t} assigned by the logit rule (8). This specification serves a dual purpose: it isolates the role of the shared switching mechanism by removing the expectation channel entirely so that any comovement between ξ_t and ζ_t must originate from the logit and it provides a baseline against which the off-diagonal specifications of Sections 4.2 and 4.3 can be compared.

Consider the trend-following matrix

$$\mathbf{\Phi}^1 = \begin{pmatrix} 1.2 & 0 \\ 0 & 1.2 \end{pmatrix}. \tag{17}$$

Since $\phi^1_{12} = \phi^1_{21} = 0$, the pricing equation for each asset depends only on its own lagged deviation. The two markets are coupled exclusively through the logit rule, which assigns a single population share n_{1t} governing both assets simultaneously.

Since $\mathbf{\Phi}^1 = \mathrm{diag}(1.2, 1.2)$ and $A = (n_1^{\mathrm{FSS}}/R)\mathbf{\Phi}^1$ by (14), the block A is itself diagonal with identical entries $n_1^{\mathrm{FSS}}\phi^1_{ii}/R$. Its two eigenvalues therefore coincide and reach the unit circle simultaneously when $n_1^{\mathrm{FSS}} = R/\phi^1_{ii} = 1.1/1.2 \approx 0.917$, which through the logit yields $\beta_{\mathrm{c}} \approx 2.40$.

Time series. Figure 2 displays the price deviations and population shares at $\beta = 3.6$, well above the stability boundary. The system exhibits quasi-periodic orbits characterized by explosive rises followed by sharp reversals, the bubble-and-crash pattern documented in the single-asset HAM literature (Brock and Hommes, 1998; Hommes, 2013). The two deviations ξ_t and ζ_t display the same qualitative dynamics, bubbles and crashes occurring at the same times, but with persistently different amplitudes, the difference being determined by the initial conditions.

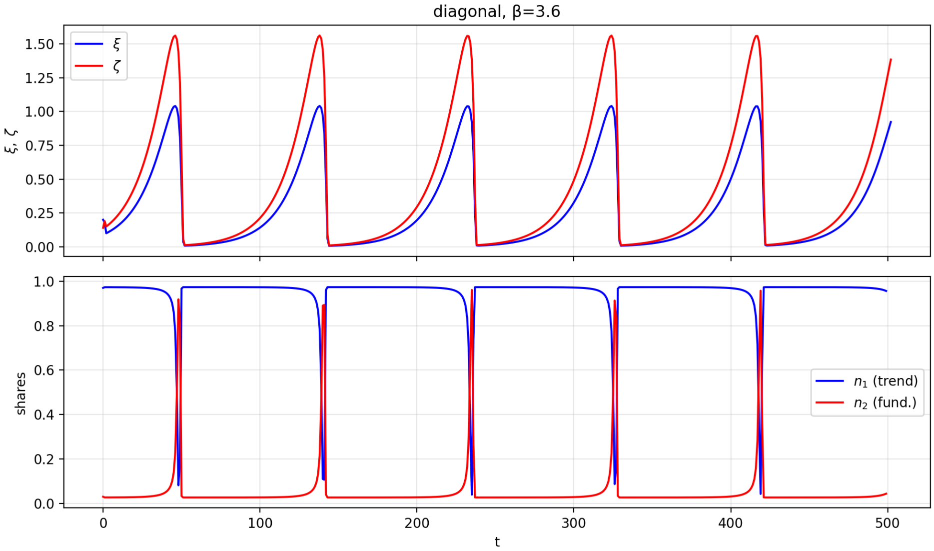

Figure 2: Price deviations ξ_t, ζ_t (top panel) and population shares n_{1t}, n_{2t} (bottom panel) for the diagonal specification (17) at $\beta = 3.6$. Trajectories remain distinct, quasi-periodic orbits, exhibiting the classical bubble-and-crash pattern.

The comovement of ξ_t and ζ_t is notable because no element of the expectation structure links the two assets. A counterfactual simulation in which agents switch strategies independently for each market shows that the correlation drops from $\hat{\rho} = 1.00$ to $\hat{\rho} = 0.27$ (see Appendix F for the full analysis). The near perfect comovement therefore originates entirely from the shared logit: when agents revise their strategy they do so for both assets at the same time, imposing a common regime on both pricing equations.

Bifurcation structure. Figure 3 reports the bifurcation diagram for ξ_t and ζ_t as β varies over $[1.0, 4.5]$. For $\beta < \beta_c$ the FSS is the unique attractor; at $\beta = \beta_c$ both eigenvalues of A reach $+1$ simultaneously, and a continuum of non-fundamental steady states emerges along a circle in the plane (ξ, ζ). The economic mechanism is the following: as β rises the logit responds more sharply to differences in realized net profit. At the FSS both rules forecast correctly and earn the same gross profit, so the fitness gap reduces to the information cost: trend followers pay nothing while fundamentalists pay C_2. Trend followers are therefore favoured at every $\beta > 0$ and their share $n_1^{\mathrm{FSS}} = (1 + e^{-\beta\Delta C})^{-1}$ grows. At $\beta_c \approx 2.40$ it reaches $n_c \approx 0.917$, the extrapolative feedback exactly offsets discounting, and the fundamental price stops being attracting.

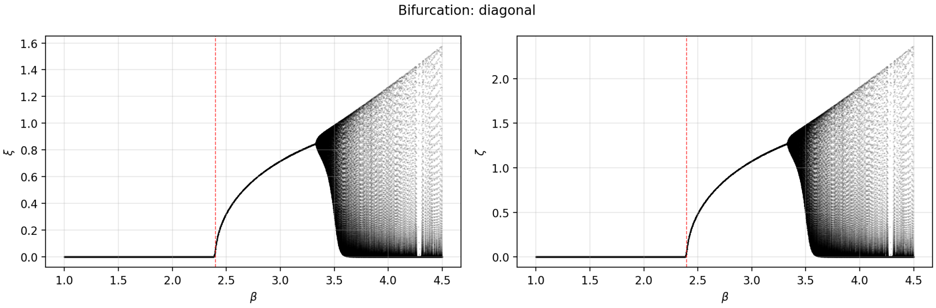

Figure 3: Bifurcation diagram for ξ_t (left) and ζ_t (right) as a function of $\beta \in [1.0, 4.5]$, diagonal specification (17). The dashed red line marks $\beta_c \approx 2.40$.

Figure 4 shows the moduli of the two eigenvalues of the 2×2 block A evaluated at the FSS as a function of β. In the diagonal specification the eigenvalue coincide at $n_1^{\text{FSS}} \phi_{ii}^1 / R$ for both i, so the curves overlap: they grow monotonically with β through the logit and both cross $+1$ at $\beta_c \approx 2.40$.

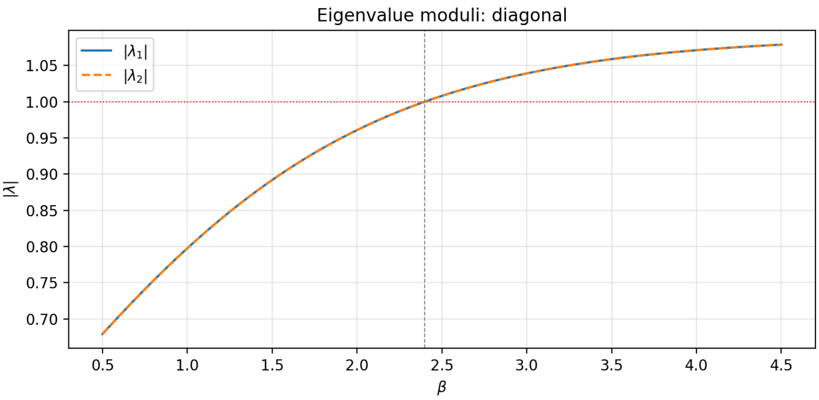

Figure 4: Eigenvalue moduli of the 2×2 block A evaluated at the FSS as a function of β, diagonal specification (17). The dashed grey line marks β_c where the eigenvalues cross the unit circle.

The transition from the stable non-fundamental fixed point to the quasi-periodic regime visible in Figure 2 requires a second bifurcation whose classification demands the full six-dimensional Jacobian evaluated at the non-fundamental fixed point. We locate this fixed point numerically for each value of $\beta > \beta_c$ and compute the 6×6 Jacobian by finite differences (see Appendix G for the numerical procedure and the complete eigenvalue trajectories).

Figure 5 reports the moduli of the non-trivial eigenvalues of this Jacobian for $\beta > \beta_c$, distinguishing real eigenvalues (squares) from complex conjugate pairs (circles). For $\beta_c < \beta < 2.88$ all non-trivial eigenvalues are real and lie strictly inside the unit disc, so the non-fundamental fixed point is locally stable. At $\beta \approx 2.88$ two real eigenvalues merge into a complex pair whose modulus grows monotonically and crosses the unit circle at $\beta_{\mathrm{NS}} \approx 3.33$. This is a Neimark-Sacker bifurcation: the non-fundamental fixed point loses stability and an invariant close curve arises, corresponding to the quasi-periodic bubble-and-crash orbits observed in Figure 2.

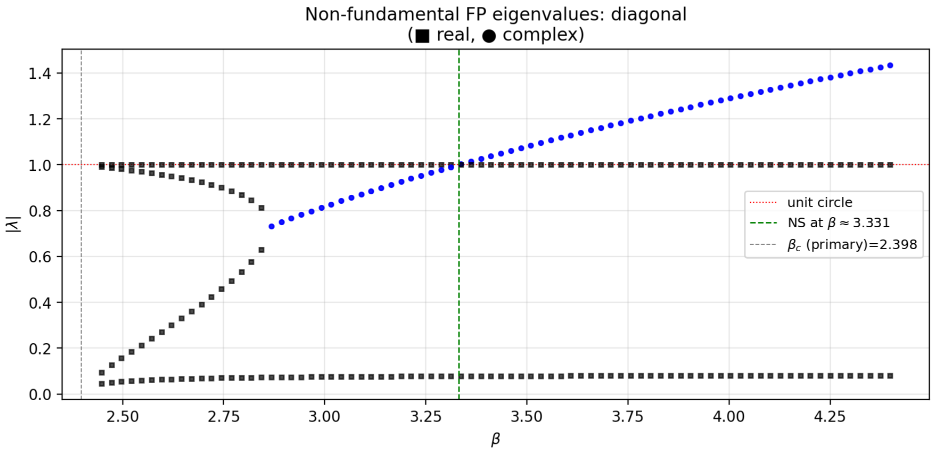

Figure 5: Non-trivial eigenvalue moduli of the 6×6 Jacobian at the non-fundamental fixed point as a function of β, diagonal specification (17). Squares: real eigenvalues; circles: complex conjugate pairs. The dashed green line marks $\beta_{\mathrm{NS}} \approx 3.33$ where the complex eigenvalue crosses the unit circle producing a Neimark-Sacker bifurcation.

The complete bifurcation sequence for the diagonal benchmark is: (degenerate) pitchfork at the FSS ($\beta_c \approx 2.40$) $\rightarrow$ stable non-fundamental fixed point $\rightarrow$ Neimark-Sacker ($\beta_{\mathrm{NS}} \approx 3.33$) $\rightarrow$ quasi-periodic dynamics. The gap between the pitchfork bifurcation and the Neimark-Sacker bifurcation is $\Delta\beta \approx 0.93$.

The non-fundamental fixed point (selected at the symmetric representative $\xi^{**} = \zeta^{**}$, see Appendix G for the fixed-point continuum in the diagonal case) has a unit eigenvalue in the differential direction $(1, -1)'$, the direction in which the two deviations move apart, while the common direction is damped. The consequences of this structure for the stochastic system are examined in Section 5.1 and Appendix H.

4.2 Symmetric cross-asset expectations

The simplet deviation from the diagonal benchmark is introducing equal off-diagonal entries $\phi^1_{12} = \phi^1_{21} = \phi > 0$, so that asset's trend-following forecast extrapolates equally from the other's lagged deviation activating the cross-asset expectation channel. The non-trivial off-diagonal elements increase the spectral radius of $\mathbf{\Phi}^1$ relative to the diagonal benchmark, making the stability bound of Proposition 3.1 tighter (lowering β_c), i.e. the pitchfork bifurcation occurs earlier.

For the numerical analysis we adopt

$$\mathbf{\Phi}^1 = \begin{pmatrix} 1.2 & 0.1 \\ 0.1 & 1.2 \end{pmatrix}, \tag{18}$$

so that each asset's trend-following forecast extrapolates symmetrically from the other's lagged deviation. From the stability analysis, $\beta_\mathrm{c} \approx 1.70$: the off-diagonal entries lower the threshold by 29% relative to the diagonal case.

Time series. Figure 6 shows the system at $\beta = 2.4$. Two properties distinguish this case from the diagonal benchmark. First, the deviations ξ_t and ζ_t overlap exactly: the time-averaged absolute difference is $\overline{|\xi_t - \zeta_t|} = 0.000$, indicating perfect synchronization despite different initial conditions. The matrix $\mathbf{\Phi}^1$ in (18) has eigenvalues 1.3 and 1.1, with eigenvectors $(1,1)'$ and $(1,-1)'$. Since $A = (n_1^{\mathrm{FSS}}/R)\mathbf{\Phi}^1$, the block A has the same eigenvectors. The eigenvalue associated with $(1,1)'$ is the larger of the two and is the first to cross the unit circle as β increases. At the bifurcation the system therefore destabilizes along the direction $\xi = \zeta$: both deviations grow together. Conversely, the eigenvalue associated with $(1,-1)'$, the direction along which ξ and ζ move apart, equals $\lambda \approx 0.846$ at $\beta = \beta_\mathrm{c}$, and remains strictly inside the unit circle. Any difference $\xi_t - \zeta_t$ introduced by the initial conditions therefore shrinks geometrically over time, and the long-run orbit satisfies $\xi_t = \zeta_t$ exactly.

Second, the oscillations in the population share n_{1t} preceding each crash are sharper than in the diagonal case. The largest eigenvalue of $\mathbf{\Phi}^1$ is 1.3 versus 1.2 in the diagonal specification: the effective trend-following rule amplifies mispricings more strongly per iteration when cross-asset feedback is present. Larger mispricings produce larger swings in realized profits (7), so the logit (8) switches faster between the two strategies.

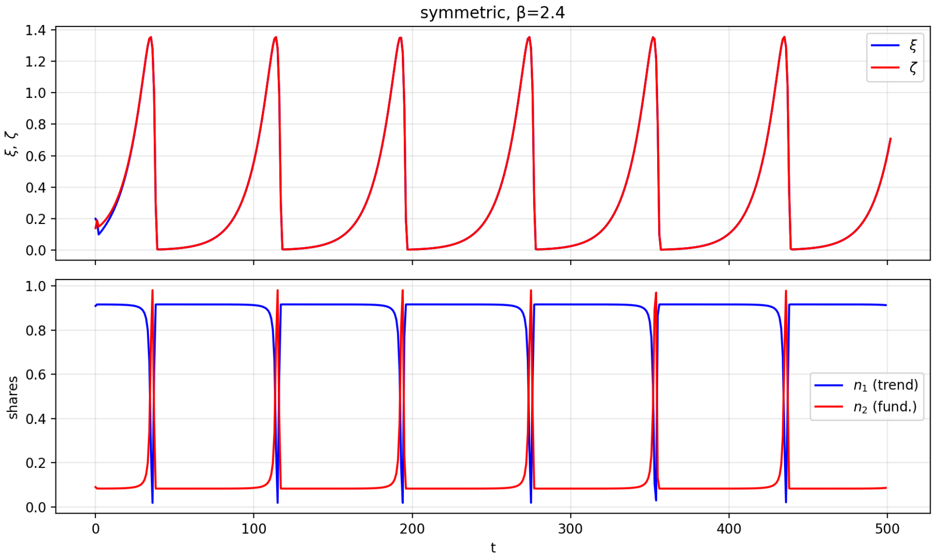

Figure 6: Price deviations ξ_t, ζ_t (top panel) and population shares n_{1t}, n_{2t} (bottom panel) for the symmetric specification (18) at $\beta = 2.4$. Trajectories overlap in quasi-periodic orbits, $\beta = 2.4$ is smaller than the one chosen for 2 to show the classical bubble-and-crash pattern.

Bifurcation structure. The bifurcation diagram (Figure 7, $\beta \in [1.0, 2.2]$) and the dynamics of the eigenvalue moduli of the 2×2 block A evaluated at the FSS, (Figure 8), confirm the pitchfork at $\beta_c \approx 1.70$.

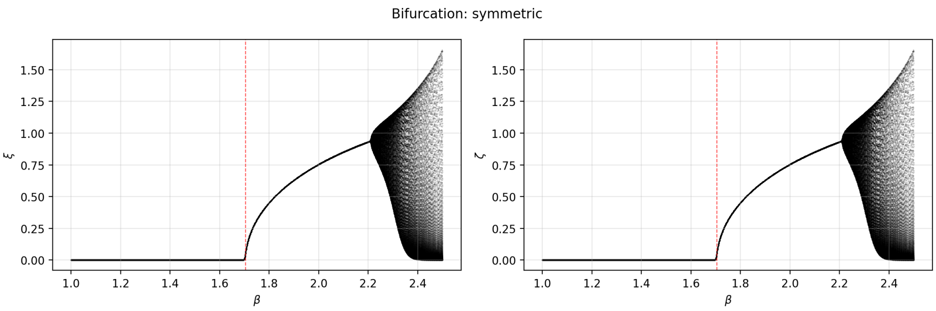

Figure 7: Bifurcation diagram for ξ_t and ζ_t, $\beta \in [1.0, 2.2]$, symmetric specification (18). The dashed red line marks $\beta_c \approx 1.70$.

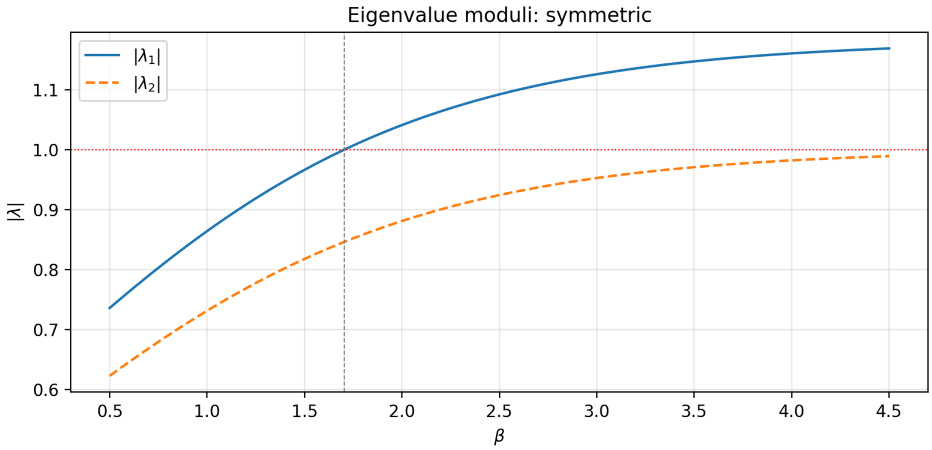

Figure 8: Eigenvalue moduli of the 2×2 block A evaluated at the FSS as a function of β, symmetric specification (18). The dashed grey line marks β_c where one eigenvalue crosses the unit circle.

The secondary bifurcation analysis (Figure 9) reveals the same qualitative pattern as the diagonal case: two real eigenvalues of the 6×6 Jacobian at the non-fundamental fixed point coalesce into a complex conjugate pair whose modulus crosses the unit circle at $\beta_{\text{NS}} \approx 2.21$. The eigenvalue along the differential direction $(1, -1)'$ remains constant at 0.846 throughout and the bifurcation is driven by the eigenvalues associated with the common direction.

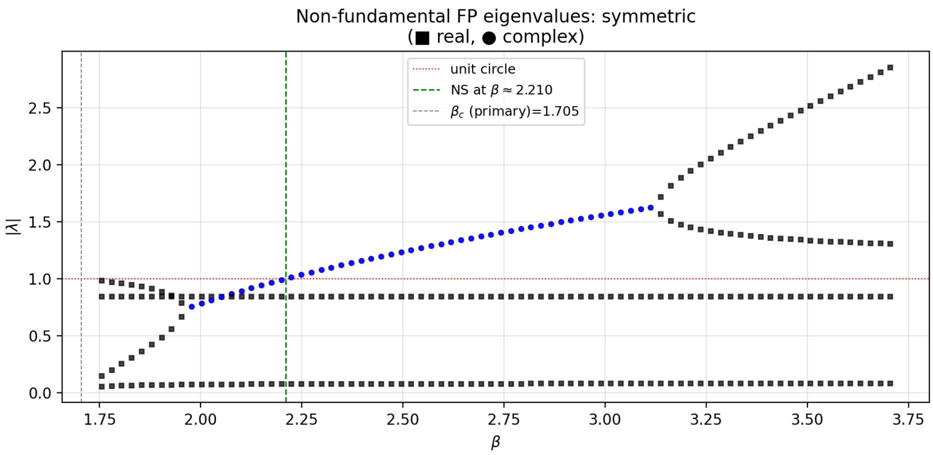

Figure 9: Non-trivial eigenvalue moduli of the 6×6 Jacobian at the non-fundamental fixed point, symmetric specification (18). Notation as in Figure 5. The dashed green line marks $\beta_{\text{NS}} \approx 2.21$ where the complex eigenvalue crosses the unit circle.

The interval between the two bifurcations ($\beta_{\mathrm{NS}} - \beta_{\mathrm{c}}$) narrows to $\Delta\beta = 0.51$, a compression of 45% relative to the diagonal benchmark. Cross-asset expectations therefore have a twofold destabilizing effect: they lower the threshold at which the FSS loses stability and they reduce the parameter range over which a non-oscillatory mispricing can persist. In contrast to the diagonal case, at the non-fundamental fixed point the differential direction is damped (eigenvalue modulus 0.846) while the common direction governs the dominant dynamics.

4.3 Asymmetric cross-asset expectations

Finally, we allow the cross-asset feedback to be asymmetric by setting

$$\mathbf{\Phi}^1 = \begin{pmatrix} 1.2 & 0.2 \\ 0.1 & 1.2 \end{pmatrix}, \tag{19}$$

so that the forecast of asset 1 extrapolates twice as strongly from the lagged deviation of asset 2 as the reverse ($\phi^1_{12} = 0.2$ versus $\phi^1_{21} = 0.1$). The largest eigenvalue of $\mathbf{\Phi}^1$ is $1.2 + \sqrt{0.02} \approx 1.341$, yielding $\beta_{\mathrm{c}} \approx 1.52$. The percentage reductions in β_{c} relative to the diagonal benchmark are 29% for the symmetric specification and 37% for the asymmetric one; moving from the symmetric to the asymmetric specification accounts for a further 11% reduction relative to the symmetric threshold itself.

Time series. Figure 10 shows the system at $\beta = 2.1$. Although $\xi_0 < \zeta_0$, the long-run amplitude ordering is reversed: asset 1 exhibits larger deviations than asset 2, with $\overline{|\xi_t|} = 0.40$ versus $\overline{|\zeta_t|} = 0.283$. The time-averaged absolute difference $\overline{|\xi_t - \zeta_t|} = 0.117$ is between the diagonal case (0.149) and the symmetric case (0.000): the asymmetric feedback partially synchronizes the two assets but cannot achieve exact convergence because $\phi^1_{12} \neq \phi^1_{21}$ breaks the invariance of the subspace $\xi = \zeta$.

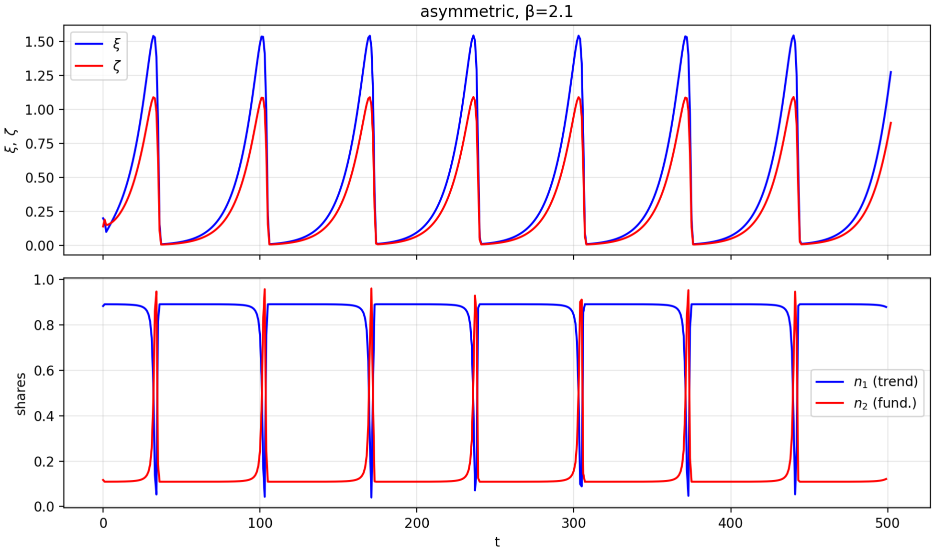

Figure 10: Price deviations ξ_t, ζ_t (top panel) and population shares n_{1t}, n_{2t} (bottom panel) for the symmetric specification (19) at $\beta = 2.1$. Trajectories recover distinct dynamics in quasi-periodic orbits.

To verify that the amplitude ordering is governed by $\mathbf{\Phi}^1$ rather than by the initial conditions, we repeat the simulation with ϕ^1_{12} and ϕ^1_{21}, keeping all other parameters identical. Table 1 reports the results: the amplitude ordering reverses almost exactly. The mechanism is direct. The coefficient ϕ^1_{12} determines how strongly the lagged deviation of asset 2 enters the forecast of asset 1. When $\phi^1_{12} > \phi^1_{21}$, asset 1 extrapolates more aggressively from asset 2, amplifying its own deviations.

	$\overline{\lvert\xi_t\rvert}$	$\overline{\lvert\zeta_t\rvert}$
$\phi^1_{12} = 0.2,\ \phi^1_{21} = 0.1$	0.400	0.283
$\phi^1_{12} = 0.1,\ \phi^1_{21} = 0.2$	0.287	0.406

Table 1: Transpose experiment for the asymmetric specification (19) at $\beta = 2.1$. Swapping the off-diagonal elements of $\mathbf{\Phi}^1$ reverses the relative amplitude of the two deviations.

Bifurcation structure. Again, the bifurcation diagram (Figure 11, $\beta \in [1.0, 2.2]$) and the dynamics of the eigenvalue moduli of the block A evaluated at the FSS, confirm the pitchfork at $\beta_c \approx 1.52$.

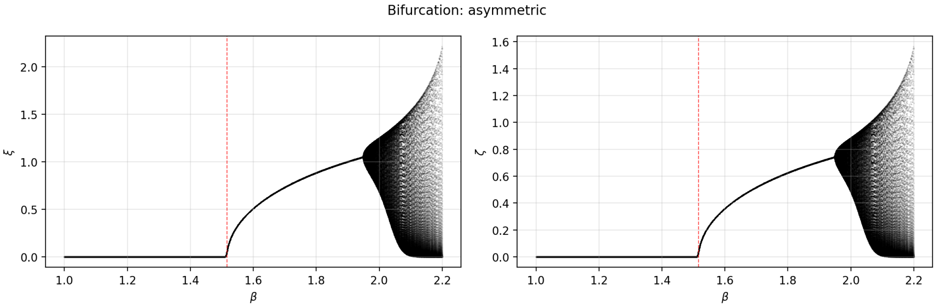

Figure 11: Bifurcation diagram for ξ_t and ζ_t, $\beta \in [1.0, 2.2]$, asymmetric specification. The dashed red line marks $\beta_c \approx 1.52$.

Similarly, the secondary bifurcation analysis (Figure 12) yields a Neimark-Sacker bifurcation at $\beta_{\text{NS}} \approx 1.95$, following the same eigenvalue coalescence pattern documented for specifications (17) and (18).

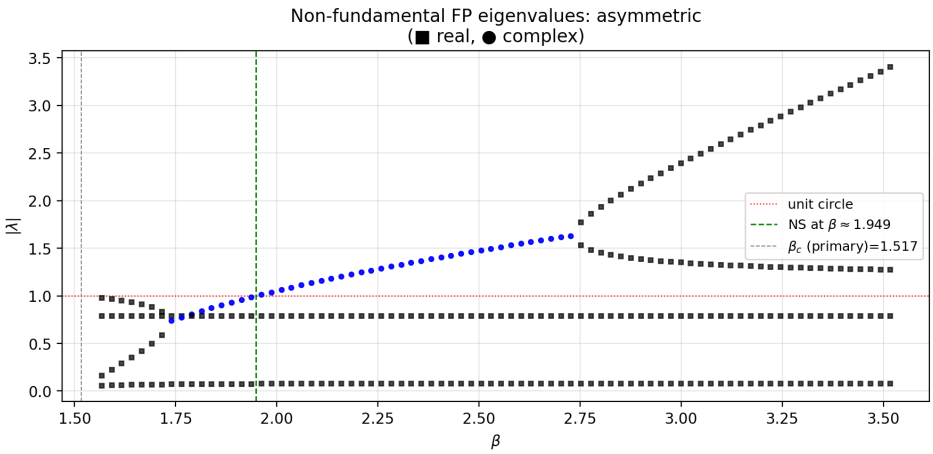

Figure 12: Non-trivial eigenvalue moduli of the 6×6 Jacobian at the non-fundamental fixed point, asymmetric specification. Notation as in Figure 5. The dashed green line marks $\beta_{\text{NS}} \approx 1.95$ where the complex eigenvalue crosses the unit circle.

The gap between the two bifurcations narrows further to $\Delta\beta = 0.43$, less than half that of the diagonal benchmark.

4.4 Summary from the numerical study

Table 2 collects the main quantitative results across the three specifications.

	(17)	(18)	(19)
β_{c} (Pitchfork)	2.40	1.70	1.52
β_{NS} (Neimark-Sacker)	3.33	2.21	1.95
$\Delta\beta = \beta_{\mathrm{NS}} - \beta_{\mathrm{c}}$	0.93	0.51	0.43
$\overline{\lvert\xi_t - \zeta_t\rvert}$	0.149	0.000	0.117

Table 2: Summary of the deterministic analysis. The convergence metric $\overline{\lvert\xi_t - \zeta_t\rvert}$ is the time-averaged absolute difference between the two price deviations, evaluated beyond the transient.

Three findings emerge. First, cross-asset expectations compress the bifurcation structure. Off-diagonal elements that are at most 17% of the diagonal entries reduce $\Delta\beta$ from $0.93 \to 0.43$, a compression exceeding 50%. Both the primary threshold β_{c} and the secondary threshold β_{NS} decrease monotonically as the spectral radius of $\mathbf{\Phi}^1$ increases, but β_{c} decreases faster than β_{NS}, so the stable non-fundamental regime shrinks.

Second, the route to complex dynamics is robust across specifications: a pitchfork bifurcation at the FSS is followed by a Neimark-Sacker bifurcation at the non-fundamental fixed point, giving rise to quasi-periodic orbits. The invariant closed curve born at the Neimark-Sacker bifurcation corresponds to the bubble-and-crash dynamics visible in the time series.

Third, the degree of synchronization between ξ_t and ζ_t is governed by the symmetry properties of $\mathbf{\Phi}^1$. In the diagonal case, comovement arises exclusively from the shared switching mechanism ($\hat{\rho} = 1.00$ under shared switching versus $\hat{\rho} = 0.27$ under independent switching). Symmetric off-diagonal elements reinforce this comovement to exact convergence by making the subspace $\xi = \zeta$ invariant. Asymmetric off-diagonal elements produce partial convergence and determine the relative amplitude of the two deviations: the asset whose forecast extrapolates more aggressively from the other develops larger long-run swings, as confirmed by the transpose experiment (Table 1).

5 Behavioral correlation

The deterministic analysis of Sections 4.4 establishes that cross-asset expectations compress the bifurcation structure and produce synchronization between the two price deviations. We now study whether this mechanism survives the introduction of exogenous noise. The central question is then whether cross-asset expectations amplify the realized correlation between the two assets beyond the correlation implied by their fundamentals.

Setup of the stochastic dynamical system. We add a correlated noise term to the pricing equations (10):

$$\begin{pmatrix} \xi_t \\ \zeta_t \end{pmatrix} = \frac{1}{R} \sum_h n_{ht} \mathbf{\Phi}^h \begin{pmatrix} \xi_{t-1} \\ \zeta_{t-1} \end{pmatrix} + \boldsymbol{\varepsilon}_t, \tag{20}$$

where $\boldsymbol{\varepsilon}_t = L\mathbf{e}_t$, with $\mathbf{e}_t \sim N(\mathbf{0}, \sigma^2 I_2)$ and L is the Cholesky factor of the correlation matrix $\left(\begin{smallmatrix} 1 & \varrho \\ \varrho & 1 \end{smallmatrix}\right)$. The parameter ϱ governs the exogenous fundamental correlation between the two assets; σ controls the noise scale. The noise can be interpreted as correlated shocks to the fundamental price processes, or equivalently as correlated approximation errors in the agents' common estimate of the fundamental values. Throughout the baseline analysis we set $\sigma = 0.01$ and $\varrho = 0.1$. Sensitivity to both parameters is examined in Appendix I.

For each parameter configuration $(\beta, \mathbf{\Phi}^1, \sigma, \varrho)$, we iterate the stochastic system (20) for $T = 2000$ time steps, discard the first 1000 as transient, and compute the Pearson correlation $\hat{\rho}(\xi, \zeta)$ on the remaining 1000 steps tail. Each configuration is replicated $M = 200$ times with independent noise draws. Reported statistics are the cross-replication mean $\hat{\rho}$ and its standard error $\mathrm{se} = s/\sqrt{M}$.

Correlation amplification. We study the properties of the stochastic system focusing on the examples 4.1 and 4.2 from the numerical section. Figure 13 reports the mean realized correlation $\hat{\rho}(\beta)$ for specifications (17) and (18), together with 90% percentile bands across the M replications. Vertical lines mark the pitchfork threshold β_{c} and the Neimark-Sacker threshold β_{NS} from the deterministic analysis.

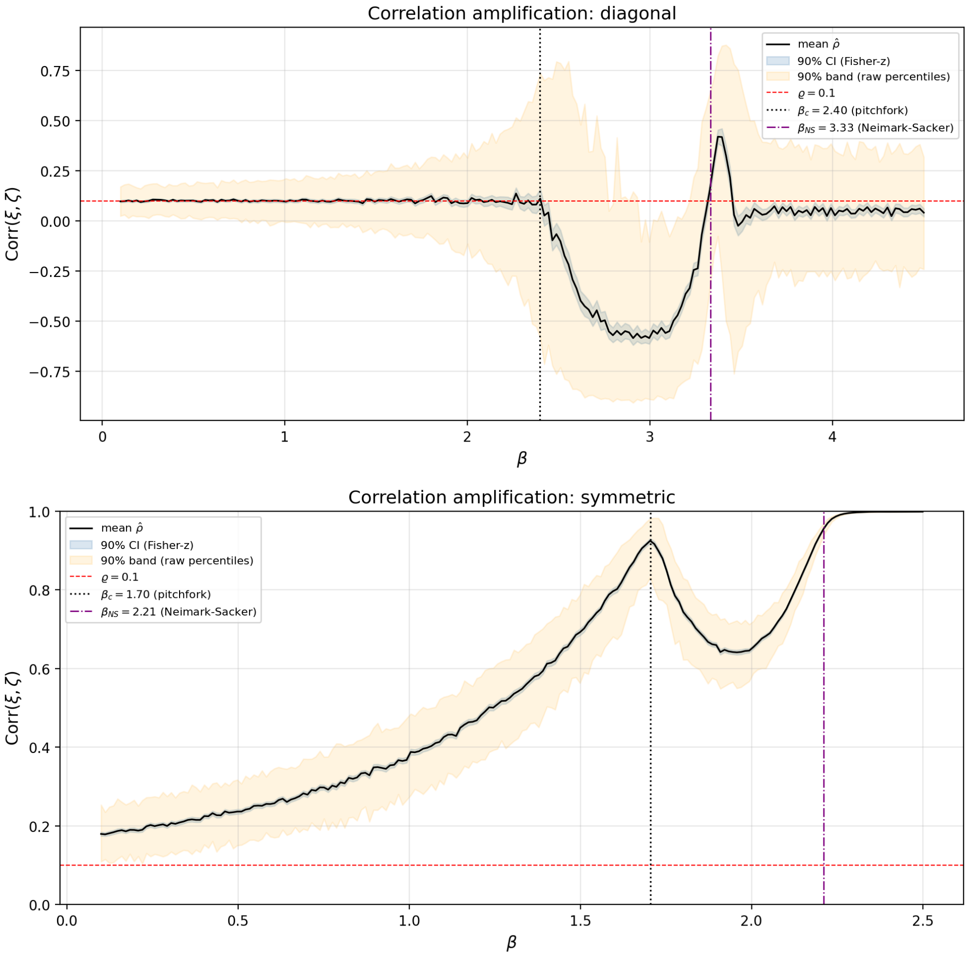

Figure 13: Mean realized correlation $\hat{\rho}(\xi, \zeta)$ as a function of β, with 90% Fisher z confidence bands (blue) and 90% raw percentile bands (orange). Top: specification (17). Bottom: specification (18). Dashed red: exogenous correlation $\varrho = 0.1$. Dotted grey: β_c. Dash-dot purple: β_{NS}. Under diagonal expectations $\hat{\rho}$ follows ρ below β_c, while symmetric cross-asset feedback lifts $\hat{\rho}$ to ≈ 0.93 at β_c, an excess of 0.83 over the fundamental baseline.

The two panels present a sharp contrast. For specification (17), the mean correlation remains indistinguishable from the fundamental level ϱ for all $\beta < \beta_c$ where β_c is exactly the bifurcation of value of β for the diagonal regime. Above β_c a regime of negative mean correlation appears ($\hat{\rho} \approx -0.58$), with a wide percentile band ($[-0.90, +0.15]$) indicating that the sign of the correlation is sensitive to the particular noise draw. The mechanism behind this sign reversal is examined in Section 5.1 and Appendix H.

For specification (18), the mean correlation rises from $\hat{\rho} \approx 0.18$ at low β to a peak of $\hat{\rho} \approx 0.93$ at $\beta = \beta_c$, an excess of 0.83 over the fundamental baseline $\varrho = 0.1$ (se $= 0.004$). Already at low values of the intensity of choice, such as $\beta \approx 0.5$, well below the pitchfork bifurcation, we observe an excess correlation of 0.14 (se < 0.005). The excess correlation increases monotonically until it reaches a peak exactly at the bifurcation value β_c. Above β_c, the correlation dips to approximately 0.64 before recovering toward unity beyond β_{NS}; the mechanism behind this non-monotonicity is examined in Section 5.1.

The off-diagonal elements of $\mathbf{\Phi}^1$ are therefore the decisive input: without cross-asset expectations, no amplification occurs and the correlation can even turn negative.

5.1 Non-monotonicity of the realized correlation

The mean realized correlation between the two assets in the symmetric specification is non-monotonic in the intensity of choice β. As shown in the lower panel of Figure 13, $\hat{\rho}$ rises sharply as β approaches the pitchfork threshold, peaks at $\hat{\rho} \approx 0.927$ (se $= 0.005$) near $\beta_c \approx 1.70$, then declines over the interval $\beta_c < \beta < \beta_{NS}$ to a local minimum of $\hat{\rho} \approx 0.631$ (se $= 0.005$) at $\beta \approx 1.95$, before recovering toward unity beyond $\beta_{NS} \approx 2.21$. The dip is present at every fundamental correlation level tested (Table 3) and its location is stable across ϱ, as shown in Figure 14.

ϱ	$\hat{\rho}$ at peak	$\hat{\rho}$ at min	difference
0.0	0.900	0.577	0.323
0.1	0.927	0.631	0.296
0.3	0.948	0.748	0.200
0.5	0.965	0.836	0.129

Table 3: Post-bifurcation dip in mean correlation for specification (18). The peak occurs at $\beta \approx 1.71$ and the trough at $\beta \approx 1.95$ across all ϱ. Each entry is the mean over $M = 100$ replications; standard errors are below 0.006 throughout.

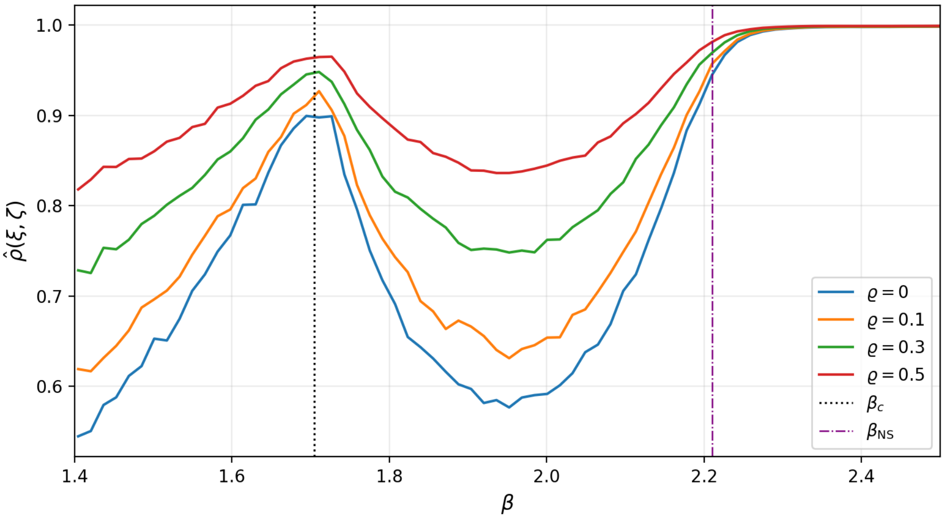

Figure 14: Mean realized correlation $\hat{\rho}(\xi, \zeta)$ for $\varrho \in \{0, 0.1, 0.3, 0.5\}$, specification (18), $\beta \in [1.4, 2.5]$. Dotted grey: $\beta_{\mathrm{c}} \approx 1.70$, pitchfork bifurcation. Dash-dot purple: $\beta_{\mathrm{NS}} \approx 2.21$ Neimark-Sacker bifurcation.

The mechanism can be traced to the eigenvalue structure of the Jacobian at the non-fundamental fixed point. Figure 15 displays the mean correlation alongside the non-trivial eigenvalue moduli of the 6×6 Jacobian over $\beta \in (\beta_{\mathrm{c}}, 2.5]$. The eigenvalue trajectories begin at $\beta_{\mathrm{c}} \approx 1.70$ (the pitchfork bifurcation) because the non-fundamental fixed point does not exist below the pitchfork.

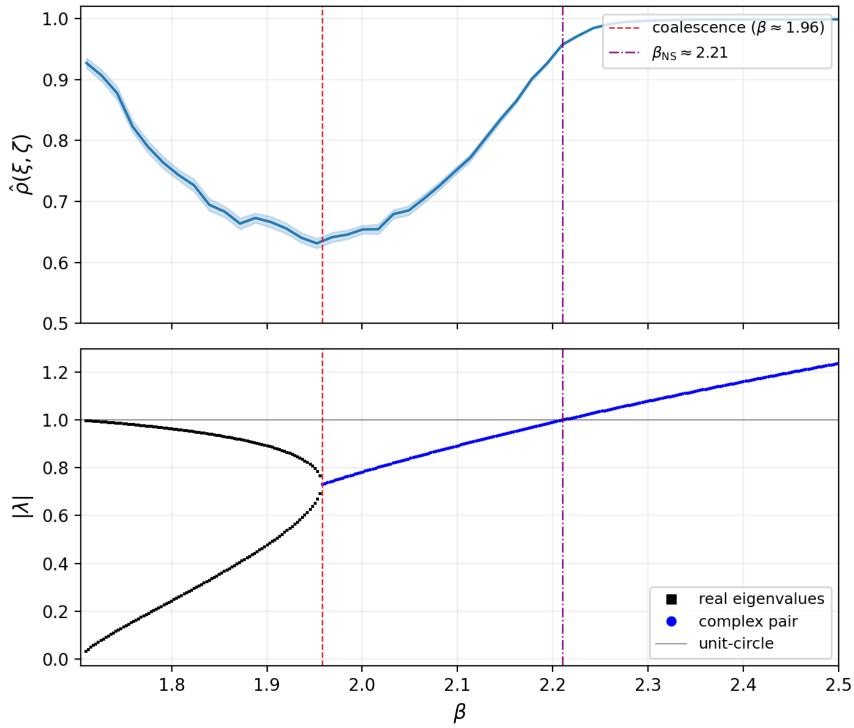

Figure 15: Top: mean realized correlation $\hat{\rho}(\xi, \zeta)$ with 90% confidence band, specification (18). Bottom: non-trivial eigenvalue moduli of the 6×6 Jacobian at the non-fundamental fixed point. Squares: real eigenvalues. Circles: complex conjugate pair. Grey line: eigenvalue pinned at $n_1^{\mathrm{FSS}} \approx 0.846$. Dashed red: eigenvalue coalescence ($\beta \approx 1.96$). Dash-dot purple: $\beta_{\mathrm{NS}} \approx 2.21$.

Just above β_c, the dominant eigenvalue has modulus ≈ 0.998: perturbations from the fixed point decay very slowly. Noise shocks therefore produce persistent fluctuations in both ξ_t and ζ_t. Because the symmetric matrix $\mathbf{\Phi}^1$ propagates each asset's shock into the other's forecast, these fluctuations are strongly correlated across assets. As β increases, two real eigenvalues of the Jacobian converge: the dominant one falls from 0.998 to 0.766 while a second rises from 0.033 to 0.692. The fixed point becomes more stable, the orbit concentrates more around it, and the time series variation is increasingly driven by the independent component of the noise rather than by the shared deterministic response. The correlation declines.

At $\beta \approx 1.96$, the realized correlation reaches its minimum in the range between β_c and β_{NS}, the two real eigenvalues merge into a complex conjugate pair at modulus 0.732. This is the point of fastest perturbation decay, and it coincides with the correlation dip: the local minimum lies at $\beta \approx 1.95$, within grid precision of the point where the complex pair emerges. Beyond the coalescence, the complex pair's modulus rises toward the unit circle, which it crosses at β_{NS}. Perturbations decay more slowly, the shared oscillatory response to shocks grows, and the correlation recovers. After β_{NS} the fixed point is unstable, the system moves onto a quasi-periodic attractor of increasing amplitude, and $\hat{\rho}$ approaches unity.

Two facts support the argument. First, a higher ϱ places a floor under $\hat{\rho}$: at $\varrho = 0.5$ the dip is only 0.13 (Table 3), because even the independent noise component retains substantial positive correlation. Second, the noise scale sensitivity analysis (Appendix I) shows that at $\beta = 2.0$ (near the minimum), increasing σ from 0.001 to 0.1 raises the correlation from 0.65 to 0.88: stronger noise overwhelms the fine structure near the coalescence.

The diagonal specification (17) also displays a decline in mean correlation above β_c, but the decline continues into the negative region ($\hat{\rho} \approx -0.58$ near $\beta \approx 2.9$). The reason lies in the eigenvector structure at the non-fundamental fixed point. In both specifications the fixed point has $\xi^* = \zeta^*$, but the directions that are stabilized differ. Under (18), the pitchfork occurs along the common direction $(1, 1)'$, and the differential direction $(1, -1)'$ is damped (eigenvalue modulus 0.846). Common perturbations persist longer than differential ones, so the correlation stays positive. Under (17), the situation is reversed: the Jacobian at the non-fundamental fixed point has a unit eigenvalue whose eigenvector is the differential direction, while the common direction is damped by a complex pair of modulus 0.819. The differential perturbations therefore accumulate under repeated noise, the common ones decay, and $\text{Cov}(\xi_t, \zeta_t)$ turns negative (Appendix H).

5.2 Decomposition of comovement

The amplification documented in the previous paragraph could operate through two channels: the off-diagonal elements of $\mathbf{\Phi}^1$, which link each asset's forecast to the other's lagged deviation, and the shared logit rule (8), which forces both assets to be governed by the same population share n_{1t}. To separate these channels we construct three configurations of the model, all under specification (18) with $\sigma = 0.01$ and $\varrho = 0.1$: the full model specification $\mathbf{\Phi}^1 = \left(\begin{smallmatrix} 1.2 & 0.1 \\ 0.1 & 1.2 \end{smallmatrix}\right)$, shared switching, correlated noise; diagonal expectations, where $\mathbf{\Phi}^1$ is replaced with $\text{diag}(\mathbf{\Phi^1}) = \left(\begin{smallmatrix} 1.2 & 0 \\ 0 & 1.2 \end{smallmatrix}\right)$, shared switching, same noise; independent switching, same $\text{diag}(\mathbf{\Phi}^1)$, but each asset switches independently based on its own profit, same noise.

For each replication, the three configurations receive the same noise sequence (common random numbers), so that difference in realized correlation can only be explained by the model structure. The *expectation channel* is $\Delta_{\text{exp}} = \hat{\rho}_{\text{full}} - \hat{\rho}_{\text{diag}}$; the *switching channel* is $\Delta_{\text{switch}} = \hat{\rho}_{\text{diag}} - \hat{\rho}_{\text{indep}}$; the residual $\hat{\rho}_{\text{indep}}$ is the *noise baseline*.

Table 4 reports the results at selected β values.

β	$\hat{\rho}_{\text{full}}$	$\hat{\rho}_{\text{diag}}$	$\hat{\rho}_{\text{indep}}$	Δ_{exp}	Δ_{switch}
0.50	0.239	0.101	0.101	0.138	0.000
0.85	0.326	0.101	0.101	0.225	0.000
1.20	0.472	0.099	0.099	0.372	0.000
1.70	0.921	0.097	0.097	0.824	0.000
2.00	0.655	0.107	0.107	0.548	0.000
2.40	0.998	0.058	0.054	0.940	0.004

Table 4: Decomposition of realized correlation for specification (18). Each entry is the mean over $M = 200$ replications with common random numbers. Standard errors are below 0.005 for all entries at $\beta \leq 2.0$ and below 0.031 at $\beta = 2.4$.

The expectation channel accounts for the entire excess correlation at every β: Δ_{exp} ranges from 0.14 at $\beta = 0.5$ to 0.94 at $\beta = 2.4$. The switching channel is indistinguishable from zero at all β values below β_{NS} and reaches at most 0.004 at the highest value tested. The noise baseline tracks $\varrho = 0.1$ closely, drifting below it only at $\beta = 2.4$ where the large deterministic attractor absorbs part of the noise variance.

This result complements the deterministic comparison between the diagonal and symmetric specifications. In the diagonal benchmark, the two assets are linked only by the shared switching rule: this is enough to generate synchronized regimes in the deterministic system, but it does not generate excess realized correlation (Table 4). Replacing shared switching with independent switching leaves the realized correlation essentially unchanged. The difference therefore comes from the expectation matrix, not from the switching rule: under the symmetric specification, the off-diagonal elements of $\mathbf{\Phi}^1$ transmit shocks from one asset into the forecast of the other, creating a joint propagation mechanism; under the diagonal specification, that propagation channel is absent. Appendix H shows that this distinction also appears in the local dynamics around the non-fundamental fixed point: in the diagonal case differential perturbations are not damped, whereas in the symmetric case they are. This is why the expectation channel accounts for the excess correlation in Table 4, while the switching channel is negligible.

5.3 Summary of the analysis of excess correlation

The stochastic analysis yields three results.

First, cross-asset expectations amplify the realized correlation well beyond the exogenous baseline. Under specification (18) with $\varrho = 0.1$, the excess correlation $\hat{\rho} - \varrho$ reaches 0.83 at β_c (se = 0.004). The effect is present even at low β (excess

$= 0.14$ at $\beta = 0.5$) and is robust to changes in the noise scale: across a two orders of magnitude range of σ, the correlation at $\beta \leq 1.0$ varies by less than 0.005 (Appendix I). The amplification does not require exogenous correlation: at $\varrho = 0$, the mean realized correlation is 0.90 at β_{c} (Appendix J). Under diagonal expectations (17), by contrast, no amplification occurs for $\beta < \beta_{\mathrm{c}}$; above β_{c} mean correlation is reverse and turns negative.

Second, the amplification operates entirely through the expectation channel. The decomposition of Section 5.2 shows that replacing the symmetric (18) with its diagonal (17) eliminates the excess correlation, while replacing the shared logit with independent switching has no effect. The eigenvector analysis of Appendix H identifies the structural reason: the off-diagonal elements of $\mathbf{\Phi}^1$ damp the differential component of the two-asset system, keeping the common variation dominant. Without them, the differential component carries a unit eigenvalue and accumulates under noise, driving the correlation toward zero or below.

Third, the mean correlation is non-monotone in β: it peaks near β_{c}, dips in the region $\beta_{\mathrm{c}} < \beta < \beta_{\mathrm{NS}}$ and recovers beyond β_{NS}. The local minimum coincides with the coalescence of two real eigenvalues into a complex pair (Section 5.1) and is present at every exogenous correlation level tested (Table 3).

At high β the correlation approaches unity, but this should not be interpreted as evidence that the two assets become identical. The mean absolute gap $\overline{|\xi_t - \zeta_t|}$ remains bounded away from zero (approximately 0.020 in the post bifurcation region for specification (18)); what drives $\hat{\rho} \to 1$ is the growth of the common deterministic component relative to the noise, a signal-to-noise ratio effect documented in Appendix K.

6 Conclusion

This paper proposes a model that describes a mechanism through which trading behavior with heterogeneous expectations introduces excess covariance between financial assets. We extend the Brock & Hommes framework to a market with two risky assets where forecasts for one asset depends on the lagged price deviations of both through a forecasting matrix $\mathbf{\Phi}^1$. Its off-diagonal elements introduce cross-asset expectations as a distinct source of endogenous comovement.

The deterministic analysis establishes that cross-asset expectations are destabilizing: off-diagonal elements that are small relative to the diagonal entries substantially lower the stability threshold of the fundamental steady state and compress the region in which a stable non-fundamental fixed point can persist. The bifurcation route, pitchfork followed by Neimark-Sacker, is robust across the three specifications we examine, and the symmetry properties of $\mathbf{\Phi}^1$ govern the degree of synchronization between the two price deviations: symmetric off-diagonal elements make the system symmetric in the two assets, so that the two deviations converge exactly once they meet, while asymmetric elements produce partial convergence and determine which asset develops larger long-run swings.

The stochastic analysis shows that these properties carry over to the noisy system. Cross-asset expectations amplify the realized correlation far beyond the exogenous noise correlation and we can attribute this amplification entirely to the expectation channel rather than to the shared switching mechanism. The realized correlation is non-monotone in the intensity of switching: it peaks near the pitchfork threshold, dips where the non-fundamental fixed point is most stable, and recovers beyond the Neimark-Sacker threshold. We trace this pattern to the eigenvalue structure of the Jacobian at the non-fundamental fixed point, specifically the coalescence of two real eigenvalues into a complex pair. A change of coordinates into common and differential components reveals that the off-diagonal elements of $\mathbf{\Phi}^1$ are necessary not only for amplifying the correlation but also for keeping it positive: without them, the differential component carries a unit eigenvalue and accumulates under noise.

Our finding that cross-asset expectation formation alone can generate realized price correlation far in excess of fundamental correlation offers a mechanism for the excess comovement documented since Pindyck and Rotemberg (1990, 1993) and for the location-of-trade effects in dual-listed companies (Froot and Dabora, 1999). Acknowledging category and habitat effects (Barberis et al., 2005) and the impact of shared information in the pricing of different assets (Veldkamp, 2006), our model shows that a joint extrapolative forecasting rule is by itself sufficient.

Whether the mechanism identified here is quantitatively relevant for observed asset correlations is an open question that would require calibration to the data. The analytical tractability of the model, however, makes the cross-asset expectation channel easy to isolate and the results suggest that the structure of forecasting rules is a quantitatively relevant determinant of price comovement.

Appendix

A Conditional variance and F.O.C.s

The difference between realized and expected wealth at $t+1$ is

$$W_{t+1} - \mathrm{E}_{ht}[W_{t+1}] = \\ z_t(p_{t+1} + d_{t+1} - \mathrm{E}_{ht}[p_{t+1} + d_{t+1}]) + v_t(q_{t+1} + c_{t+1} - \mathrm{E}_{ht}[q_{t+1} + c_{t+1}]).$$

Setting $A_{t+1} \equiv p_{t+1} + d_{t+1}$ and $B_{t+1} \equiv q_{t+1} + c_{t+1}$ for compactness, the conditional variance of next-period wealth is

$$\begin{aligned} \mathrm{Var}_{ht}[W_{t+1}] &= E_{ht}\left[(z_t(A_{t+1} - E_{ht}[A_{t+1}]) + v_t(B_{t+1} - E_{ht}[B_{t+1}]))^2\right] \\ &= z_t^2 \,\mathrm{Var}_{ht}[A_{t+1}] + v_t^2 \,\mathrm{Var}_{ht}[B_{t+1}] + 2z_t v_t \,\mathrm{Cov}_{ht}[A_{t+1}, B_{t+1}]. \end{aligned} \tag{21}$$

Differentiating (1) with respect to z_t and v_t and setting both derivatives to zero gives the system

$$\mathrm{E}_{ht}[p_{t+1} + d_{t+1}] - Rp_t - az_t\sigma_R^2 - av_t\rho\sigma_R\sigma_G = 0, \tag{22}$$

$$\mathrm{E}_{ht}[q_{t+1} + c_{t+1}] - Rq_t - av_t\sigma_G^2 - az_t\rho\sigma_R\sigma_G = 0, \tag{23}$$

which yields the demand functions (2). Solving the 2×2 system for (z_{ht}, v_{ht}) as functions of prices and expectations gives

$$\begin{cases} z_{ht} = \dfrac{E_{ht}[p_{t+1} + d_{t+1}]\sigma_G - E_{ht}[q_{t+1} + c_{t+1}]\rho\sigma_R - Rp_t\sigma_G + Rq_t\rho\sigma_R}{a\sigma_R^2\sigma_G(1-\rho^2)}, \\ v_{ht} = \dfrac{E_{ht}[q_{t+1} + c_{t+1}]\sigma_R - E_{ht}[p_{t+1} + d_{t+1}]\rho\sigma_G - Rq_t\sigma_R + Rp_t\rho\sigma_G}{a\sigma_R\sigma_G^2(1-\rho^2)}. \end{cases}$$

B Cancellation of the fundamental correlation

We show that under zero net supply ($z_S = v_S = 0$) the fundamental correlation ρ drops out of the pricing equations. Starting from the solved demands, market clearing requires $\sum_h n_{ht} z_{ht} = 0$ and $\sum_h n_{ht} v_{ht} = 0$. After multiplying through by the common denominators, the system becomes

$$\begin{cases} Rp_t = \displaystyle\sum_h n_{ht}\,\mathrm{E}_{ht}[p_{t+1} + d_{t+1}] - \frac{\rho\sigma_R}{\sigma_G}\sum_h n_{ht}\,\mathrm{E}_{ht}[q_{t+1} + c_{t+1}] + Rq_t\frac{\rho\sigma_R}{\sigma_G}, \\ Rq_t = \displaystyle\sum_h n_{ht}\,\mathrm{E}_{ht}[q_{t+1} + c_{t+1}] - \frac{\rho\sigma_G}{\sigma_R}\sum_h n_{ht}\,\mathrm{E}_{ht}[p_{t+1} + d_{t+1}] + Rp_t\frac{\rho\sigma_G}{\sigma_R}. \end{cases}$$

Substituting the second equation into the first to eliminate q_t:

$$R p_t = \sum_h n_{ht}\,\mathrm{E}_{ht}[p_{t+1} + d_{t+1}] - \frac{\rho\sigma_R}{\sigma_G}\sum_h n_{ht}\,\mathrm{E}_{ht}[q_{t+1} + c_{t+1}]$$
$$+ \frac{\rho\sigma_R}{\sigma_G}\left(\sum_h n_{ht}\,\mathrm{E}_{ht}[q_{t+1} + c_{t+1}] - \frac{\rho\sigma_G}{\sigma_R}\sum_h n_{ht}\,\mathrm{E}_{ht}[p_{t+1} + d_{t+1}] + R p_t \frac{\rho\sigma_G}{\sigma_R}\right).$$

The terms in $\sum_h n_{ht}\,\mathrm{E}_{ht}[q_{t+1} + c_{t+1}]$ cancel. Collecting the remaining terms:

$$R p_t\left(1 - \rho^2\right) = \sum_h n_{ht}\,\mathrm{E}_{ht}[p_{t+1} + d_{t+1}]\left(1 - \rho^2\right).$$

Since $\rho^2\sigma_G\sigma_R < 1$, we can divide both sides to obtain

$$p_t = \frac{1}{R}\sum_h n_{ht}\,\mathrm{E}_{ht}[p_{t+1} + d_{t+1}].$$

An identical argument applied to q_t yields the second equation in (3). The fundamental correlation ρ is therefore irrelevant for pricing under zero net supply: any observed comovement must originate from the expectation structure.

C Excess return decomposition

Define $\mathbf{x}_t = (\xi_t, \zeta_t)'$, $\mathbf{x}_t = (p_t^*, q_t^*)'$ and $\mathbf{y}_t = (d_t, c_t)'$. The total return on the two assets in terms of price levels is $\mathbf{x}_t + \mathbf{x}_t^* + \mathbf{y}_t$. The vector of excess returns can be decomposed as

$$\boldsymbol{x}_t + \boldsymbol{x}_t^* + \boldsymbol{y}_t - R\left(\boldsymbol{x}_{t-1} + \boldsymbol{x}_{t-1}^*\right) =$$
$$\boldsymbol{x}_t - R\,\boldsymbol{x}_{t-1} + \underbrace{\boldsymbol{x}_t^* + \boldsymbol{y}_t - E_{t-1}[\boldsymbol{x}_t^* + \boldsymbol{y}_t]}_{\equiv\boldsymbol{\delta}_t} + \underbrace{E_{t-1}[\boldsymbol{x}_t^* + \boldsymbol{y}_t] - R\,\boldsymbol{x}_{t-1}^*}_{=0},$$

where the last term vanishes by the definition of fundamental prices. In the deterministic skeleton $\delta_t = 0$, the excess return reduces to $\mathbf{x}_t - R\mathbf{x}_{t-1}$, which is the expression entering the profit measure (6).

D Proof of Proposition 3.1

Proof of Proposition 3.1. Write $\nu \equiv n_1^{\mathrm{FSS}}/R > 0$ for brevity. Under $\boldsymbol{\Phi}^2 = \mathbf{0}$ and (14), $A = \nu\,\boldsymbol{\Phi}^1$, so $T_A = \nu T$ and $D_A = \nu^2 D$. The FSS is locally asymptotically stable iff both eigenvalues of A lie strictly inside the unit disc, equivalently the Jury conditions hold:

(i) $1+\nu T+\nu^2 D>0$, (ii) $1-\nu T+\nu^2 D>0$, (iii) $1-\nu^2 D>0$.

Since $T, D, \nu > 0$, (i) is automatic. Condition (iii) is equivalent to

$$\nu < \tfrac{1}{\sqrt{D}}. \tag{24}$$

For (ii), consider $f(\nu) = 1-\nu T+\nu^2 D$ as a quadratic in ν with discriminant T^2-4D.

Case 1: $T^2 \le 4D$. Then f has no real roots and $f(0) = 1 > 0$, so $f > 0$ for all ν; (ii) is automatic. Only 24 binds.

Case 2: $T^2 > 4D$. The roots $\nu_\pm = (T \pm \sqrt{T^2-4D})/(2D)$ are both positive (since $T > 0$) and $f > 0$ for $\nu < \nu_-$ and for $\nu_+ < \nu$. The branch containing $\nu = 0$ is $(0, \nu_-)$, so (ii) is equivalent to

$$\nu < \nu_- = \tfrac{T-\sqrt{T^2-4D}}{2D}. \tag{25}$$

We now show that in this case the bound (25) is tighter than (24), i.e. $\nu_- < 1/\sqrt{D}$. Multiplying both sides by $2D > 0$ and rearranging,

$$\nu_- < \tfrac{1}{\sqrt{D}} \iff T-2\sqrt{D} < \sqrt{T^2-4D}.$$

By the case hypothesis $T^2 > 4D$ and $T > 0$, both sides are non-negative ($T > 2\sqrt{D}$), so squaring preserves the inequality:

$$T^2-4T\sqrt{D}+4D < T^2-4D \iff 8D < 4T\sqrt{D} \iff T > 2\sqrt{D} \iff T^2 > 4D,$$

which holds by hypothesis. Hence (25) binds.

Both cases are summarized by

$$\nu < \min\left\{\tfrac{1}{\sqrt{D}},\ \tfrac{T-\sqrt{T^2-4D}}{2D}\right\}.$$

Multiplying through by R yields the threshold n_c in (15).

For (16): $n_1^{FSS} = (1+e^{-\beta\Delta C})^{-1}$ is strictly increasing in β for $\Delta C > 0$, with inverse $\beta = (\Delta C)^{-1}\ln(n_1^{FSS}/(1-n_1^{FSS}))$. Setting $n_1^{FSS} = n_c$ gives β_c. □

E Gershgorin bound on stability

The Gershgorin circle theorem provides an alternative sufficient condition for the stability of the FSS that is simpler to state, though more conservative than the exact Schur-Cohn conditions of Proposition 3.1.

Every eigenvalue of J_{FSS} lies in at least one of the six discs $\mathcal{D}(a_{ii}, R_i)$, where a_{ii} is the i-th diagonal entry and $R_i = \sum_{j \neq i} |a_{ij}|$ is the absolute row sum of the off-diagonal entries of the i-th row. For the Jacobian 12 the six discs are:

$$\mathcal{D}_1 = \mathcal{D}(a_{11}, |a_{12}|), \quad \mathcal{D}_4 = \mathcal{D}(a_{22}, |a_{21}|), \quad \mathcal{D}_k = \mathcal{D}(0,1) \text{ for } k \in \{2,3,5,6\}.$$

The four discs $\mathcal{D}_k$ centered at the origin with radius 1 contain the four zero eigenvalues. A sufficient condition for the two remaining eigenvalues to lie isnide the unit circle is that $\mathcal{D}_1$ and $\mathcal{D}_4$ are contained in the open unit disc, which requires

$$|a_{11}| + |a_{12}| < 1 \qquad \text{and} \qquad |a_{22}| + |a_{21}| < 1.$$

Under (14) with $\mathbf{\Phi}^2 = \mathbf{0}$, these become

$$n_1^{FSS} < \frac{R}{|\phi^1_{11}| + |\phi^1_{12}|} \qquad \text{and} \qquad n_1^{FSS} < \frac{R}{|\phi^1_{22}| + |\phi^1_{21}|}, \tag{26}$$

or equivalently, in terms of β,

$$\beta < \frac{1}{\Delta C} \ln\left(\frac{\bar{n}}{1-\bar{n}}\right), \qquad \bar{n} \equiv \min\left\{\frac{R}{|\phi^1_{11}| + |\phi^1_{12}|}, \frac{R}{|\phi^1_{22}| + |\phi^1_{21}|}\right\}.$$

The Gershgorin bound $\bar{n}$ is always at least as restrictive as the exact threshold n^* from Proposition 3.1: $\bar{n} \leq n^*$. For diagonal $\mathbf{\Phi}^1$ (no cross-asset feedback), the two bounds coincide. When off-diagonal elements are present and asymmetric ($|\phi^1_{12}| \neq |\phi^1_{21}|$), the Gershgorin bound is striclty conservative. For instance, with $\mathbf{\Phi}^1 = \left(\begin{smallmatrix} 1.2 & 0.2 \\ 0.1 & 1.2 \end{smallmatrix}\right)$, the Gershgorin bound gives $\bar{n} \approx 0.786$ ($\beta^*_G \approx 1.3$), while the exact Schur-Cohn threshold is $n^* \approx 0.82$ ($\beta_c \approx 1.52$).

F Counterfactual switching experiment

To isolate the role of the shared logit in generating comovement between ξ_t and ζ_t, we compare the baseline model, in which agents adopt a single strategy for both assets, with a counterfactual in which each asset has an independent switching mechanism. In the counterfactual, agents evaluate the profitability of their strategy separately for each market and may adopt different rules in different markets: an agent can be a trend follower in asset 1 and a fundamentalist in asset 2. All other parameters are identical to the diagonal baseline specification (17) at $\beta = 3.6$, above β_{NS}.

On the deterministic attractor, shared switching gives a sample correlation between the two deviations of $\hat{\rho} = 1.00$; under independent switching it falls to $\hat{\rho} = 0.27$. The synchronisation of the deterministic orbit therefore originates entirely from the shared logit: when agents revise their strategy they do so for both assets at once, imposing a common regime on both pricing equations even when $\mathbf{\Phi}^1$ is diagonal. This is a property of the deterministic skeleton alone. Once fundamental noise is added, the diagonal specification behaves differently: with $\mathbf{\Phi}^1$ diagonal there is no cross-asset restoring force, the differential component carries a unit eigenvalue (Appendix H), and the realized correlation turns negative. The shared logit synchronizes the common deterministic orbit but does not couple the two assets' responses to noise.

G Secondary bifurcation analysis

For each $\beta > \beta_c$ we locate the non-fundamental fixed point $x^{**} = (\xi^{**}, \zeta^{**})'$ by solving the two-dimensional fixed-point condition numerically and compute the 6×6 Jacobian $DF(\boldsymbol{s}^{**})$ by centred finite differences. The eigenvalue structure at the non-fundamental fixed point has the same qualitative form in all three specifications: two eigenvalues are near zero (from the lag structure), one small negative eigenvalue is close to zero throughout, one eigenvalue is constant across β, and the remaining two eigenvalues evolve with β and are responsible for the Neimark-Sacker bifurcation. The constant eigenvalue and the evolving pair differ across specifications.

For the diagonal specification (17), the constant eigenvalue equals 1.000 at every β above β_c. This reflects the fact that when both diagonal entries of $\mathbf{\Phi}^1$ are equal, the fixed-point condition places no restriction on the ratio ξ^{**}/ζ^{**}: any direction is a valid fixed point. A perturbation that changes this ratio therefore moves the system to a neighbouring fixed point and neither grows nor decays. Eigenvalue moduli are invariant across this set; we use the symmetric representative $\xi^{**} = \zeta^{**}$ (obtained by initializing the solver at a symmetric guess), at which the unit-eigenvalue eigenvector lies along the differential direction $(1, -1)'$. The two evolving eigenvalues are real just above β_c (moduli 0.981 and 0.159 at $\beta = 2.50$), converge as β increases, coalesce into a complex conjugate pair at $\beta \approx 2.88$, and cross the unit circle at $\beta_{\mathrm{NS}} \approx 3.33$.

For the symmetric specification (18), the constant eigenvalue equals 0.846. This is the eigenvalue associated with the differential direction $(1, -1)'$: perturbations that push the two deviations apart contract at rate 0.846 per period. The two evolving eigenvalues follow the same pattern, real, converging, coalescing at $\beta \approx 1.96$, and crossing the unit circle at $\beta_{\mathrm{NS}} \approx 2.21$. No eigenvalue equals unity at any β: the non-fundamental fixed point is isolated (unlike in the diagonal case), so there is no neutral direction.

For the asymmetric specification (19), the constant eigenvalue equals 0.789, again in the direction that separates the two assets. The complex pair crosses the unit circle at $\beta_{\mathrm{NS}} \approx 1.95$.

The constant eigenvalue has a transparent origin. At the non-fundamental fixed point, the fixed-point condition requires x^{**} to be an eigenvector of $\mathbf{\Phi}^1$ with eigenvalue R/n_1^{**}, where n_1^{**} is the trend-follower share at the fixed point. The direction orthogonal to x^{**} corresponds to the other eigenvalue of $\mathbf{\Phi}^1$, call it λ_2. The constant eigenvalue of the 6×6 Jacobian in this direction equals $\lambda_2/(R/n_1^{**}) = \lambda_2/\lambda_1$, the ratio of the two eigenvalues of $\mathbf{\Phi}^1$. For the symmetric specification this gives $1.1/1.3 = 0.846$; for the asymmetric, $1.059/1.341 = 0.789$; for the diagonal, $1.2/1.2 = 1.000$.

Figures 5, 9, and 12 display the non-trivial eigenvalue moduli for the three specifications.

H Dynamics at the non-fundamental fixed point

The post bifurcation behaviour of the realized correlation can be understood through a change of coordinates that separates the joint dynamics of (ξ_t, ζ_t) into a common and a differential component. Define

$$c_t = \frac{\xi_t + \zeta_t}{2}, \qquad d_t = \frac{\zeta_t - \xi_t}{2},$$

so that $\xi_t = c_t - d_t$ and $\zeta_t = c_t + d_t$. The component c_t captures movements in which the two assets move together; d_t captures movements in which they move apart. In terms of these components the covariance decomposes as

$$\mathrm{Cov}(\xi_t, \zeta_t) = \mathrm{Var}(c_t) - \mathrm{Var}(d_t). \tag{27}$$

The realized correlation is positive when the common variation dominates and negative when the differential variation dominates.

Such decomposition corresponds to rewriting the 6×6 Jacobian at the non-fundamental fixed point in the bases of the common direction $(1,1)'$ and the differential direction $(1,-1)'$. Let $\mathbf{s} = (\xi_t, \xi_{t-1}, \xi_{t-2}, \zeta_t, \zeta_{t-1}, \zeta_{t-2})'$ denote the state vector and $J = DF(s^{**})$ the Jacobian at the non-fundamental fixed point. Applying the change of coordinates to all three lag levels defines a transformation matrix T such that the new state $\tilde{\mathbf{s}} = (c_t, c_{t-1}, c_{t-2}, d_t, d_{t-1}, d_{t-2})'$ evolves under $\tilde{J} = T^{-1}JT$. For both the diagonal and the symmetric specifications (using the symmetric representative $\xi^{**} = \zeta^{**}$ in the diagonal case), the transformed Jacobian $\tilde{J}$ is exactly block-diagonal:

$$\tilde{J} = \begin{pmatrix} J_c & 0 \\ 0 & J_d \end{pmatrix},$$

where J_c is the 3×3 block governing the common component and J_d is the 3×3 block governing the differential component. The two components therefore evolve independently near the fixed point: shocks to c_t do not affect d_t and viceversa.

For specification (17) at $\beta = 3.0$, the eigenvalues of the two blocks are

$$\lambda(J_c) = \{0.819, 0.819, 0.075\}, \qquad \lambda(J_d) = \{1.000, 0, 0\}.$$

The common block is stable: its dominant eigenvalues (the complex pair of modulus 0.819) ensure that common perturbations decay. The differential block contains a unit eigenvalue, so differential perturbations neither grow nor decay. Each noise shock adds a component in the differential direction that persists indefinitely, while the common component of the same shock is damped away. Over many periods the accumulated differential variation exceeds the common variation, $\mathrm{Var}(d_t) > \mathrm{Var}(c_t)$, and by (27) the covariance turns negative.

For specification (18) at $\beta = 2.0$, the eigenvalues are

$$\lambda(J_c) = \{0.783, 0.783, 0.074\}, \qquad \lambda(J_d) = \{0.846, 0, 0\}.$$

Both blocks are stable throughout this region, so both variances are finite; the covariance sign is set by which direction accumulates more noise variance, which in turn depends on how close each modulus is to one. The differential modulus is fixed at 0.846. Above β_c the common modulus first declines, dips below 0.846, and then rises again toward the Neimark–Sacker crossing. While it sits below 0.846 the differential direction is the more persistent one, $\mathrm{Var}(d_t)$ gains on $\mathrm{Var}(c_t)$, and the realized correlation falls to its minimum; once the common modulus returns back above 0.846, $\mathrm{Var}(c_t)$ dominates again and the correlation recovers. The dip is therefore the interval over which the common amplification is temporarily weaker than the fixed differential mode.

The difference between the two specifications reduces to a single structural property. In the diagonal case, each asset's forecast depends only on its own lagged deviation, so nothing restores the ratio ξ_t/ζ_t once noise has perturbed it: the differential block carries a unit eigenvalue, $\mathrm{Var}(d_t)$ grows without bound, and the correlation turns negative. In the symmetric case, the off-diagonal elements of $\mathbf{\Phi}^1$ couple the two forecasts and pin the differential modulus at 0.846, strictly below one; $\mathrm{Var}(d_t)$ stays finite, so even at the dip the correlation only weakens and never changes sign. This is why cross-asset expectations are necessary not only for amplifying the correlation but for keeping it positive.

I Robustness to the noise scale

To verify that the amplification result is not an artefact of small noise, we repeat the analysis for specification (18) across six noise scales spanning two orders of magnitude: $\sigma \in \{0.001, 0.005, 0.01, 0.02, 0.05, 0.1\}$, with $\varrho = 0.1$ throughout.

	σ					
β	0.001	0.005	0.01	0.02	0.05	0.1
0.5	0.237	0.241	0.241	0.236	0.240	0.237
1.0	0.379	0.381	0.375	0.380	0.377	0.376
1.5	0.696	0.689	0.698	0.695	0.685	0.638
1.7	0.955	0.930	0.927	0.909	0.853	0.764
2.0	0.652	0.652	0.652	0.661	0.785	0.880
2.4	1.000	1.000	0.998	0.995	0.985	0.998

Table 5: Mean realized correlation for specification (18) across noise scales σ, with $\varrho = 0.1$. Each entry is the mean over $M = 150$ replications. Standard errors are below 0.006 throughout.

For $\beta \leq 1.0$ the realized correlation is invariant to the noise scale: across the full σ range the mean $\hat{\rho}$ varies by less than 0.007. The amplification at low β is therefore a property of the linearized dynamics around the FSS, not a consequence of negligible noise. At $\beta \approx \beta_c$ the correlation decreases with σ, from 0.955 at $\sigma = 0.001$ to 0.764 at $\sigma = 0.1$, but the excess $\hat{\rho} - \varrho = 0.66$ at $\sigma = 0.1$ remains large. The non-monotonic dip at $\beta = 2.0$ is smoothed by large noise: correlation rises from 0.65 at $\sigma = 0.001$ to 0.88 at $\sigma = 0.1$, consistent with the interpretation in Section 5.1 that larger noise hides the fine structure near the eigenvalue coalescence.

J Robustness to the exogenous correlation

We repeat the correlation-amplification analysis for specification (18) with $\varrho \in \{0, 0.1, 0.3, 0.5\}$. Table 6 reports the mean realized correlation at β_c for each value.

ϱ	$\hat{\rho}$ at β_c	excess $\hat{\rho} - \varrho$
0.0	0.900	0.900
0.1	0.927	0.827
0.3	0.945	0.645
0.5	0.963	0.463

Table 6: Mean realized correlation at $\beta = \beta_c$ for specification (18) under different exogenous correlation levels. Each entry is the mean over $M = 100$ replications (se < 0.006).

The amplification does not require exogenous correlation: at $\varrho = 0$, the mean realized correlation is 0.90, generated entirely by the cross-asset expectation structure. As ϱ increases, $\hat{\rho}$ at β_c increases slightly (from 0.900 to 0.963), but the excess

$\hat{\rho} - \varrho$ decreases (from 0.900 to 0.463). The realized correlation is largely determined by the expectation structure: increasing ρ from 0 to 0.5 raises $\hat{\rho}$ by only 0.063, while the endogenous component contributes approximately 0.9 throughout. The marginal excess shrinks because $\hat{\rho}$ is bounded above by one.

K High-β synchronisation

At high β the realized correlation approaches unity for specification (18). To assess whether this reflects near-identity of the two deviations or merely a signal-to-noise ratio effect, we track two quantities across β: the mean absolute gap $\overline{|\xi_t - \zeta_t|}$ and the mean absolute level $\overline{|\xi_t|}$, both averaged over $M = 200$ replications.

For specification (18), the mean absolute gap is approximately constant at 0.020 above β_c. What changes is the scale: $\overline{|\xi_t|}$ grows from 0.011 at $\beta = 0.5$ to 0.911 at β_{NS}. The ratio $G(\beta) \equiv \overline{|\xi_t - \zeta_t|} \,/\, (\overline{|\xi_t|} + \overline{|\zeta_t|})$ therefore falls from 0.62 to 0.011, not because the gap shrinks, but because the common deterministic component grows. The two assets remain distinct processes (their gap is bounded away from zero at every β), but the shared deterministic component becomes so large relative to the noise-driven differences that the Pearson correlation approaches unity mechanically.

	$\beta = 0.5$	$\beta = \beta_c$	$\beta = \beta_{\mathrm{NS}}$	$\beta = \beta_{\max}$
(17)	0.671	0.636	0.279	0.685
(18)	0.618	0.086	0.011	0.034
(19)	0.593	0.182	0.172	0.146

Table 7: Normalized gap $G(\beta) = \overline{|\xi_t - \zeta_t|} \,/\, (\overline{|\xi_t|} + \overline{|\zeta_t|})$, averaged over $M = 200$ replications. Values near zero indicate that the common signal dominates the gap; values near $0.5 - 0.7$ indicate that the two assets follow distinct trajectories.

For specification (17), G remains above 0.27 at all β, confirming that the two assets follow distinct trajectories throughout. For specification (19), G stabilises around $0.15 - 0.18$ above β_c, reflecting the persistent amplitude asymmetry ($\overline{|\xi_t|}/\overline{|\zeta_t|} \approx 1.4$) induced by $\phi^1_{12} \neq \phi^1_{21}$.

References

Anufriev, M., G. Bottazzi, M. Marsili, and P. Pin (2012): "Excess covariance and dynamic instability in a multi-asset model," *Journal of Economic Dynamics and Control*, 36, 1142–1161, quantifying and Understanding Dysfunctions in Financial Markets.

Barberis, N., R. Greenwood, L. Jin, and A. Shleifer (2018): "Extrapolation and Bubbles," *Journal of Financial Economics*, 129, 203–227.

Barberis, N., A. Shleifer, and J. Wurgler (2005): "Comovement," *Journal of Financial Economics*, 75, 283–317.

Brock, W. and S. Durlauf (2001): "Discrete choice with social interactions," *ReStud*, 68, 235–260.

Brock, W. and C. Hommes (1997): "A rational route to randomness," *Econometrica*, 65, 1059–1095.

——— (1998): "Heterogeneous beliefs and routes to chaos in a simple asset pricing model," *Journal of Economic Dynamics and Control*, 22, 1235–1274.

Chiarella, C., R. Dieci, and L. Gardini (2005): "The Dynamic Interaction of Speculation and Diversification," *Applied Mathematical Finance*, 12, 17–52.

Chiarella, C., R. Dieci, and X.-Z. He (2007): "Heterogeneous expectations and speculative behavior in a dynamic multi-asset framework," *Journal of Economic Behavior & Organization*, 62, 408–427.

——— (2013): "Time-Varying Beta: A Boundedly Rational Equilibrium Approach," *Journal of Evolutionary Economics*, 23, 609–639.

Dieci, R. and X.-Z. He (2018): "Chapter 5 - Heterogeneous Agent Models in Finance," in *Handbook of Computational Economics*, ed. by C. Hommes and B. LeBaron, Elsevier, vol. 4 of *Handbook of Computational Economics*, 257–328.

Dieci, R. and F. Westerhoff (2006): "The Effectiveness of Keynes–Tobin Transaction Taxes When Heterogeneous Agents Can Trade in Different Markets: A Behavioral Finance Approach," *Journal of Economic Dynamics and Control*, 30, 293–322.

——— (2010): "Heterogeneous Speculators, Endogenous Fluctuations and Interacting Markets: A Model of Stock Prices and Exchange Rates," *Journal of Economic Dynamics and Control*, 34, 743–764.

Froot, K. A. and E. M. Dabora (1999): "How are stock prices affected by the location of trade?" *Journal of Financial Economics*, 53, 189–216.

Gatev, E., W. N. Goetzmann, and K. G. Rouwenhorst (2006): "Pairs Trading: Performance of a Relative-Value Arbitrage Rule," *The Review of Financial Studies*, 19, 797–827.

He, X.-Z., Y. Li, and M. Zheng (2019): "Heterogeneous agent models in financial markets: A nonlinear dynamics approach," *International Review of Financial Analysis*, 62, 135–149.

Hommes, C. (2006): "Heterogeneous Agent Models in Economics and Finance," in *Agent-based Computational Economics*, ed. by L. Tesfatsion and K. L. Judd, Amsterdam: North-Holland, vol. 2, chap. 23, 1109–1186.

——— (2013): *Behavioral Rationality and Heterogeneous Expectations in Complex Economic Systems*, CUP.

Hommes, C., H. Huang, and D. Wang (2005): "A robust rational route to randomness in a simple asset pricing model," 29, 1043–1072.

Hommes, C. and J. Vroegop (2019): "Contagion between asset markets: A two market heterogeneous agents model with destabilising spillover effects," *Journal of Economic Dynamics and Control*, 100, 314–333.

Longin, F. and B. Solnik (1995): "Is the Correlation in International Equity Returns Constant: 1960–1990?" *Journal of International Money and Finance*, 14, 3–26.

McFadden, D. L. (1981): "Structural discrete probability models derived from theories of choice," in *Structural analysis of discrete data and econometric applications*, ed. by C. Manski and D. L. McFadden, Cambridge, US: MIT Press.

Moskowitz, T. J., Y. H. Ooi, and L. Pedersen (2012): "Time series momentum," *Journal of Financial Economics*, 104, 228–250.

Pindyck, R. and J. Rotemberg (1990): "The Excess Co-movement of Commodity Prices," *Economic Journal*, 100, 1173–89.

Pindyck, R. S. and J. J. Rotemberg (1993): "The Comovement of Stock Prices," *The Quarterly Journal of Economics*, 108, 1073–1104.

Schmitt, N. and F. Westerhoff (2014): "Speculative Behavior and the Dynamics of Interacting Stock Markets," *Journal of Economic Dynamics and Control*, 45, 262–288.

Veldkamp, L. L. (2006): "Information Markets and the Comovement of Asset Prices," *The Review of Economic Studies*, 73, 823–845.

Westerhoff, F. H. (2004): "Multiasset Market Dynamics," *Macroeconomic Dynamics*, 8, 596–616.

DOCUMENTS DE TRAVAIL GREDEG PARUS EN 2026
GREDEG Working Papers Released in 2026

2026-01 Estelle Malavolti & Frédéric Marty
L'équilibre économique des aéroports secondaires européens à l'épreuve des dynamiques de concurrence fiscale

2026-02 Charlie Joyez
A New Index of Export-Import Proximity: Conceptual Foundations and Global Patterns

2026-03 Patrice Bougette & Frédéric Marty
The SCP Paradigm Revisited: What Structuralism Really Contributed to U.S. Antitrust

2026-04 Imen Bouhlel, Nathalie Lazaric & Paolo Zeppini
Competitive Diffusion and Sustainability Transitions: The Case of Plastics Recycling Technologies

2026-05 Maxime Menuet
Fractional Replicator Dynamics

2026-06 Ilona Dielen, Patrice Bougette & Christophe Charlier
A (Green) Switch in Time Saves Nine: Assessing the Environmental Damage of the European Truck Cartel

2026-07 Thibault Schrepel & Godefroy de Boiscuillé
Questioning the Digital Markets Act's Legality

2026-08 Michael Finus & Paolo Zeppini
Green Lifestyles and Social Tipping Points

2026-09 Mathieu Chevrier & Sébastien Massoni
When Does Advisor Confidence Improve Decisions? Evidence from Human and Algorithmic Advice

2026-10 Flora Bellone, Charlie Joyez & Xavier Poulet-Goffard
Tax Avoidance by Small Multinationals as a Side Effect of Anti Tax Avoidance Policy

2026-11 Nicolas Camilotto
The Trust Game: A Historical and Methodological Analysis at the Frontier of Experimental and Behavioral Economics

2026-12 Godefroy de Boiscuillé
New product liability in the Age of AI: Modernisation under a Conservative Veil

2026-13 Claudio Barbieri, Mattia Guerini & Mauro Napoletano
When Credit Growth Diverges: Common Dynamics and Regional Heterogeneity in Italy

2026-14 Pierre Boutros, Michele Pezzoni, Lionel Nesta & Sonia Paty
Information Asymmetry in the Scientific Labor Market: The Role of Relational Links

2026-15 Marie Sciaccitano & Lionel Nesta
Green Consumption and Income Elasticities: Cross-country Evidence on Environmental Engel Curves

2026-16 Hankui Wang, Jiachen Yi & Philipp Harting
The Heterogeneous Diffusion of AI: Individuals, Organisations, and Adoption Barriers

2026-17 Flora Bellone, Edwin Fourrier-Nicolaï & Simone Vannuccini
Input Trade Shocks and the Direction of Innovation

2026-18 Riccardo Sommariva & Paolo Zeppini
Heterogeneous Expectations with Multiple Risky Assets